Contrasting roles of the wheat MRC in promoting starch granule initiation in leaves and repressing the onset of B-type granule initiation in the endosperm

Jiawen Chen[1], Yi Chen[1], Alexander Watson-Lazowski[1], Erica Hawkins[1], J. Elaine Barclay[1], Brendan Fahy[1], Robin Denley Bowers[1], Kendall Corbin[2,4], Frederick J. Warren[2], Andreas Blennow[3], Cristobal Uauy[1], David Seung[1]

[1.] John Innes Centre, Norwich Research Park, Norwich, NR4 7UH, UK
[2.] Quadram Institute, Norwich Research Park, Norwich, NR4 7UQ, UK
[3.] University of Copenhagen, Thorvaldsensvej 40, 1871 Frederiksberg, Copenhagen, Denmark
[4.] Current Address: Department of Horticulture, College of Agriculture, Food and Environment, University of Kentucky, Lexington, Kentucky, USA

Address correspondence to: David.Seung@jic.ac.uk

Short title: Tissue-specific roles of MRC in granule initiation in wheat

Abstract

The spatial and temporal patterns by which starch granules initiate vary greatly between species and organs, but molecular factors that contribute to these diverse patterns are poorly understood. In wheat, the endosperm of grains contains two distinct types of starch granules, where the synthesis of large A-type granules is initiated during early grain development, followed by small B-type granules that initiate c. 10-15 days after the A-type granules, whereas the leaves contain uniformly-sized starch granules. Here, we reveal distinct organ-specific roles of the MYOSIN-RESEMBLING CHLOROPLAST PROTEIN (MRC) in regulating granule initiation in the endosperm and leaves of wheat. We isolated three independent TILLING mutants of tetraploid wheat (*Triticum turgidum* cv. Kronos) with premature stop or missense mutations in the A genome homeolog, which is the only active homeolog in tetraploid wheat due to a disruption of the B genome homeolog that occurred shortly after wheat hybridisation. The mutants had significantly smaller A-type granules and a higher relative volume of B-type granules than the wild type. Quantification of starch granule size distributions and microscopy during grain development showed that B-type granules initiated 15 - 20 dpa in the wild-type, but as early as 10 dpa in the *mrc-1* mutant, suggesting a novel role of MRC in suppressing B-type granule initiation during early grain development. By contrast, MRC has a role in promoting granule initiation in leaves, as the mutants carrying premature stop mutations in *MRC* had fewer granules per chloroplast in comparison to the wild type. Overall, these contrasting roles of MRC among wheat organs provide new insight into functional diversification of granule initiation proteins to facilitate the diverse patterns of granule initiation observed across species and organs.

46 **Introduction**

47 Starch is the major storage carbohydrate in leaves, seeds and storage organs of most plants. It
48 is synthesised in plastids as insoluble granules composed of two glucose polymers:
49 amylopectin and amylose. Amylopectin is a branched polymer with linear α-1,4-glucan
50 chains and α-1,6-branch points, and forms the semi-crystalline starch granule matrix -
51 typically constituting 70-90% *w/w* of starch (Smith and Zeeman, 2020). Amylose constitutes
52 10 - 30% *w/w* of starch and is composed primarily of long α-1,4-linked linear chains (Seung,
53 2020). The biosynthesis of the starch polymers is relatively well understood at the molecular
54 level, and is generally conserved between leaf and storage starches (Smith and Zeeman,
55 2020). However, we are only beginning to understand how starch granule formation is
56 initiated, and the factors underpinning the vast diversity in granule initiation patterns
57 observed between different organs and species (Tetlow and Emes, 2017; Seung and Smith,
58 2019; Chen et al., 2021).

59

60 A prime example of diverse granule initiation patterns between species can be observed in the
61 seed endosperms of grasses (Matsushima et al., 2013). Grass species of the Triticeae,
62 including important cereal crops such as wheat, barley and rye, have a unique bimodal size
63 distribution of starch granules in the grain endosperm – containing large flattened A-type
64 granules (20-30 µm in diameter) and small round B-type granules (2-7 µm in diameter)
65 (Howard et al., 2011). The initiation of these two different types of granules are both spatially
66 and temporally separated: A-type granules initiate in amyloplasts as early as 4 days post
67 anthesis (dpa), whereas B-type granules initiate 10-15 days after the A-type granules (i.e.,
68 around 15-20 dpa) and at least partly within amyloplast stromules that emanate from the
69 amyloplast (Parker, 1985; Bechtel et al., 1990; Langeveld et al., 2000; Howard et al., 2011).
70 This is distinct from most other grass species, which produce "compound" starch granules –
71 where multiple granules initiate early during grain development in each amyloplast and
72 eventually fuse (e.g., in rice) (Matsushima et al., 2013). Our recent work has identified
73 proteins that are important for determining the initiation of bimodal starch granules in wheat.
74 These include B-GRANULE CONTENT1 (BGC1) in wheat/*Aegilops* - which is orthologous
75 to FLOURY ENDOSPERM6 (FLO6) in barley and rice and PROTEIN TARGETING TO
76 STARCH 2 (PTST2) in Arabidopsis and *Brachypodium* (Peng et al., 2014; Saito et al., 2017;
77 Seung et al., 2017; Chia et al., 2020; Watson-Lazowski et al., 2022). BGC1 in wheat has a
78 dose-dependent effect on granule initiation, where partial reductions in gene dosage can
79 almost eliminate B-type granules without affecting A-type granule formation, whereas

complete knockout of gene function also causes defective A-type granule formation, including the formation of some compound/semi-compound granules that arise from multiple initiations (Howard et al., 2011; Chia et al., 2020; Saccomanno et al., 2022). STARCH SYNTHASE 4 (SS4) is also required for normal A-type granule formation, as in its absence, compound granules form in place of most A-type granules (Hawkins et al., 2021). The increased number of initiations per amyloplast that led to compound granule formation in these mutants were unexpected since in Arabidopsis leaves, both SS4 and PTST2 promote granule initiation, and mutants lacking either protein have reduced numbers of starch granules per chloroplast (Roldán et al., 2007; Seung et al., 2017). These observations suggest that the proteins involved in granule initiation are to some extent conserved between species and organs, but they can act differently depending on the patterns of granule initiation in the species/tissue.

To gain further insight into such differences, we explored the function of wheat MYOSIN-RESEMBLING CHLOROPLAST PROTEIN (MRC, also known as PROTEIN INVOLVED IN STARCH INITIATION, PII1) both in chloroplasts of leaves and amyloplasts of the endosperm. MRC is a long coiled-coil protein that promotes granule initiation in Arabidopsis leaves, as most chloroplasts in the *mrc* mutant contain only a single granule (Seung et al., 2018; Vandromme et al., 2019). The exact function of MRC is unknown, but it is proposed to act via an interaction with SS4 and PTST2 (Seung et al., 2018; Vandromme et al., 2019). Consistent with previous work in Arabidopsis, we found that MRC promotes starch granule initiation in wheat leaves, but we discovered an unexpected, distinct role for MRC in the temporal control of B-type granule initiation in the wheat endosperm. MRC is expressed at the early stages of grain development, and wheat *mrc* mutants have severe alterations in the starch granule size distribution relative to the wild type, with smaller A-type granules and a higher relative volume of B-type granules. We demonstrate that this phenotype arises from the early initiation of B-type granules in the mutant, suggesting MRC represses B-type granule initiation during early grain development. This novel role of MRC in the wheat endosperm demonstrates how the function of granule initiation proteins can be adapted to mediate specific patterns of granule initiation among different species/tissues.

111 **Results**

112 *The wheat orthologs of MRC are encoded on chromosomes 6A and 6D*

113 The starch granule initiation protein MRC is highly conserved among land plants (Seung et
114 al., 2018). To determine the role of MRC in wheat, we searched the wheat genome for genes
115 encoding MRC orthologs. We ran a BLASTp search using the amino acid sequence of
116 Arabidopsis MRC (*At*MRC, At4g32190) against the protein sequences from both tetraploid
117 durum wheat (Svevo v1.1)(Maccaferri et al., 2019) and hexaploid bread wheat (IWGSG
118 Chinese Spring)(Appels et al., 2018) genomes on Ensembl Plants. For hexaploid wheat
119 (*Triticum aestivum*), the two top protein hits were TraesCS6A02G180500.1 (encoded on
120 chromosome 6A) and TraesCS6D02G164600.1 (encoded on chromosome 6D), which shared
121 95% sequence identity with each other and were predicted as homeologs on Ensembl. Both
122 genes had a two-exon structure like the Arabidopsis gene (Seung et al., 2018), and were in
123 syntenic positions on the A and D genomes (Figure 1). For tetraploid durum wheat (*Triticum*
124 *turgidum*), the top protein hit was TRITD6Av1G081580.1 (encoded on chromosome 6A),
125 which was identical in nucleotide and amino acid sequence to TraesCS6A02G180500.1. To
126 determine whether these proteins were true orthologs of *At*MRC, we repeated the
127 phylogenetic analyses of MRC homologs from our previous study (Seung et al., 2018) with
128 the wheat protein sequences included. The 6A and 6D proteins clustered together on the tree,
129 distinctly within the grass clade containing the rice and maize sequences (Supplemental
130 Figure 1A). This confirms that the proteins are the wheat orthologs of MRC and will
131 hereafter be referred to as *Ta*MRC-A1 (TraesCS6A02G180500) or *Tt*MRC-A1
132 (TRITD6Av1G081580), and *Ta*MRC-D1 (TraesCS6D02G164600). Notably, we did not find
133 a full gene model for MRC on chromosome 6B, or anywhere else on the B genome, either in
134 the durum or bread wheat genome.

135

136 To investigate why no homeolog was detected on chromosome 6B, we looked at the syntenic
137 region of chromosome 6B in Chinese Spring, where there was a stretch of sequence that had
138 homology to exon 2 and the beginning of the 3'UTR (Figure 1A). Interestingly, around 14kb
139 downstream of that, there was a region highly similar to the end of the 3' UTR of *TaMRC-*
140 *A1*. We looked at the transposable element annotation of the wheat reference genome around
141 the exon 2 fragment (Daron et al., 2014), and a complete *gypsy* retrotransposon was
142 annotated between the two 3'UTR fragments (Figure 1B). Further, we identified the 5 bp
143 target site duplication (GAGAT, which is part of the 3'UTR) and the inverted terminal repeat

144 (TGTAA and TTACA at the start and end of the retrotransposon, respectively) characteristic
145 of retrotransposon insertions. Further, the distance between the 5' end of the exon 2 fragment
146 and its upstream neighbouring gene (TraesCS6B02G20500, a respiratory burst oxidase
147 homolog) was much larger than the distance between *Ta*MRC and the homeologs of the same
148 neighbouring gene on 6A and 6D, indicating a large insertion in this 6B region (Figure 1A).
149 Indeed, a fragment of another *gypsy* retrotransposon was found ca. 16 kb upstream of the
150 exon 2 fragment. Additionally, there was a sequence with homology to the 5' UTR of
151 *TaMRC-A1* (85% identity over 243 bp) just 3 bp upstream of the exon 2 fragment, which
152 suggests that there was also a ~1.3 kbp deletion (based on A genome distances) that removed
153 the some of the 5' UTR, all of exon 1, intron 1 and the start of exon 2 of *TaMRC-B1*. Similar
154 to Chinese Spring, we found identical disruptions in *TaMRC-B1* sequences with
155 retrotransposon insertions and deletions in ten additional wheat genome assemblies
156 (Walkowiak et al., 2020). Overall, it appears that a deletion and a series of transposon
157 insertions severely disrupted *MRC* on chromosome 6B in bread wheat.
158
159 Since no B genome copy was found in durum wheat either, it is likely that the disruption of
160 *MRC* on chromosome 6B preceded the second hybridisation that resulted in hexaploid wheat.
161 To further investigate when the disruption of *MRC-B1* occurred, we looked for *MRC-B1* in
162 more tetraploid wheat accessions by aligning genome sequencing reads from *Triticum*
163 *dicoccoides* (wild emmer) (n=10) and *Triticum turgidum* ssp. *durum* (pasta wheat) (n=12)
164 against the A and B-genomes of Chinese Spring (Zhou et al., 2020) (Supplemental Table 1).
165 The exon 1 deletion and the retrotransposon insertion at the 3' end were detected in all
166 accessions (except for a few lines that had poor sequencing depth in the region), suggesting
167 that *TaMRC* on 6B was disrupted before or right after the hybridization of the A and B
168 genome. To distinguish these possibilities, we examined *MRC* in *Aegilops speltoides*, the
169 diploid species thought to be most closely related to the progenitor species of the wheat B
170 genome. We ran a BLASTn search on the genome assembly of the *Aegilops speltoides*
171 accession TS01 using the coding sequence of *TaMRC-A1* (Li et al., 2022) (Supplemental File
172 1). The top hit was on chromosome 6S (homologous to chromosome 6B in wheat) with intact
173 exons one and two (97.5% sequence identity), and the translated protein sequence had 96%
174 identity to *Ta*MRC-A1 with BLASTp. Thus, it is likely that *MRC* is intact in *Aegilops*
175 *speltoides*, suggesting that the loss of the B-homeolog occurred shortly after the hybridisation
176 that gave rise to tetraploid wheat (Figure 1C). It is therefore expected that all tetraploid

177 wheats have one *MRC* homeolog (on chromosome 6A), and all hexaploids have two (on
178 chromosomes 6A and 6D).
179
180 *MRC is expressed in leaves and developing endosperm*
181 We then looked at expression data of *TaMRC* homeologs using the hexaploid wheat
182 expression browser (Borrill et al., 2016; Ramirez-Gonzalez et al., 2018). Transcripts of the
183 6A and 6D homoeologs were detected in both leaves and grains, suggesting that MRC plays a
184 role in both these tissues (Figure 2A). To obtain temporal information on MRC expression in
185 the endosperm during grain development, we performed RNAseq analysis on dissected
186 endosperms of durum wheat (*Triticum turgidum* cv. Kronos) throughout grain development.
187 The full dataset is available in our accompanying paper (Chen et al., 2022). The Kronos
188 variety was chosen as it is the genetic background of the tetraploid wheat TILLING mutants
189 characterised below. *TtMRC-A1* (TRITD6Av1G081580.1) showed a peak of expression
190 during early grain development (8 dpa), but strongly decreased in expression between 10 – 20
191 dpa (Figure 2B). It therefore appears that *MRC* is expressed in the wheat endosperm almost
192 exclusively during early grain development.
193
194 *Loss of MRC does not affect the growth of wheat plants, or grain development*
195 To study the function of MRC in wheat, we obtained mutants in durum wheat (*Triticum*
196 *turgidum* cv. Kronos) defective in *MRC*. We used the wheat *in silico* TILLING mutant
197 resource, which has an EMS-mutagenised population of Kronos with exome-capture
198 sequencing data for identification of lines with mutations of interest (Krasileva et al., 2017).
199 We obtained three mutants that were likely to cause a loss of function in *TtMRC-6A* (Figure
200 1B). The K3272 and K4681 lines contained premature stop codons in place of the 258th and
201 550th amino acids respectively. In addition, we obtained a third line that contained a missense
202 Leu289Phe mutation, which was predicted to be deleterious to protein function by SIFT
203 scoring (Ng and Henikoff, 2006). The Leu^{289} residue is highly conserved in all MRC
204 orthologs, and its mutation to a Phe residue is predicted to disrupt coiled coil formation in the
205 region of the residue (Supplemental Figure 1B). Since the 6B homoeolog of MRC has likely
206 become a pseudogene, we predicted that *TtMRC-A1* would be the only functional *MRC*
207 homeolog in tetraploid wheat. However, to rule out the possibility that the fragment of exon 2
208 on chromosome 6B affects MRC function, we also obtained the K4305 and K3078 lines
209 which contain two different premature stop codon mutations in the putative reading frame of
210 the exon. We generated the *mrc-1* lines by crossing K3272 and K3078, and isolated lines

211 homozygous for either the 6A (F_2 *aa*BB) or 6B (F_2 AA*bb*) mutation, or both (F_2 *aabb*). The
212 double mutant line was backcrossed twice to wild type, and the wild-type segregant (BC_2F_2
213 AABB) and the homozygous double mutant (BC_2F_2 *aabb*) were selected. These will be
214 hereafter referred to as BC2 AABB and BC2 *aabb*. The *mrc-2* lines were generated in the
215 same way, but the K4681 and K4305 lines were crossed and no backcrossing was done. The
216 *mrc-3* line contained the K598 missense mutation, and no crossing was conducted.
217
218 Under our growth conditions, none of the *mrc* mutant plants showed obvious differences in
219 growth or in the number of tillers per plant (Figure 3A, B, Supplemental Table 2A), and the
220 number of grains per plant did not differ in the mutants, except for a slight decrease in *mrc-3*
221 and the wild-type segregant (*mrc-1* BC2 AABB) compared to the wild type (WT) (Figure 3C,
222 Supplemental Table 2B). The morphology of the mature grains of the mutants was
223 indistinguishable from the WT (Figure 3D), and there were no differences in thousand grain
224 weight (TGW) and grain size between the WT and any of the three mutants *mrc-1, mrc-2,*
225 *mrc-3*, or between the WT and the backcrossed *mrc-1* (*mrc-1* BC2 *aabb*); but the wild-type
226 segregant (*mrc-1* BC2 AABB) had a slightly higher TGW and grain size compared to WT
227 (Figure 3E, F, Supplemental Table 2C,D). This suggests that some of the background
228 mutations in the wild-type segregant may have slightly affected grain development, but these
229 effects are small. There was no consistent effect of the independent *mrc* mutations on plant
230 growth or grain development.
231
232 *Loss of MRC greatly alters starch granule size distributions in the endosperm*
233 To determine the effect of the *mrc* mutations on starch synthesis in grains, we first measured
234 total starch content of mature grains. Starch content was largely similar between WT and the
235 *mrc* mutants. Although some pairwise comparisons showed $p<0.05$ (WT with *mrc-2* and *mrc-*
236 *3*), the confidence intervals of the difference in means still reached close to zero, suggesting
237 that any effect of the mutations was small (Figure 4A). We then looked at the number of
238 starch granules in the *mrc* mutants using a Coulter counter. The total number of granules
239 relative to grain weight (granules/mg grain) was similar between genotypes (Figure 4B).
240 However, the backcrossed *mrc-1* mutant had more starch granules per unit grain weight than
241 both the WT and the wild-type segregant, and although the non-backcrossed *mrc-1* mutant
242 was not significantly different to the WT, it trended towards having more granules per mg
243 grain. The *mrc-2* mutant also had relatively more granules than the WT, but *mrc-3* did not.
244

245 Granule size distributions were determined from the Coulter counter data by plotting the
246 percentage of starch volume in each size bin relative to the total volume of starch measured.
247 We observed clear bimodal distributions for all genotypes, with a peak corresponding to A-
248 type granules (~ 18 – 25 µm) and a peak corresponding to B-type granules (~3 – 10 µm).
249 However, the distribution profiles in the mutants were greatly altered compared to the WT,
250 with the peak corresponding to B-type granules being more prominent in the mutants (Figure
251 5A). The profiles of the backcrossed *mrc-1* lines looked similar to their non-backcrossed
252 equivalents. We fitted a bimodal log-normal distribution curve to the profiles of each sample
253 to estimate the total volume percentage of B-type granules and the mean sizes of A- and B-
254 type granules. Comparing the means of these extracted values between genotypes showed a
255 higher B-type granule percentage (by volume) for all three mutants (*mrc-1, mrc-2* and *mrc-3*)
256 compared to the WT (Figure 5B). The strongest increase was seen for *mrc-1*, and this
257 increase was consistent when comparing the double backcrossed *mrc-1* (*mrc-1* BC2 *aabb*)
258 with WT and the wild-type segregant (*mrc-1* BC2 AABB). There was a small increase in the
259 volume percentage of B-type granules in the wild-type segregant compared to the wild type,
260 but the difference was much smaller than between the other genotypes. The higher B-type
261 granule volume percentage in *mrc* mutants can be due to both an increase in B-type granule
262 size and number. The mean B-type granule size was larger for *mrc-1* (and *mrc-1* BC2 *aabb*)
263 and *mrc-2* compared to wild type, but not *mrc-3* (Figure 5D). By contrast, the mean A-type
264 granule diameter was smaller for all three mutants compared to wild type (Figure 5C). Thus,
265 the increased proportion of B-type granule volume may be due to a combination of smaller
266 A-type granules, as well as larger and/or more numerous B-type granules.
267
268 We also explored whether the *mrc* mutations affected starch granule shape. We examined
269 iodine-stained thin sections of mature grains of the *mrc* mutants using light microscopy. Like
270 the wild type, all mutants had flattened A-type and round B-type granules (Figure 6A).
271 Similarly, no defects in A- or B-type granule shape were observed in the starch granules of
272 the mutants using scanning electron microscopy (SEM) (Figure 6B). We also tested whether
273 starch polymer structure or composition was affected by mutation in MRC. The *mrc-1* mutant
274 with the strongest alteration in granule size distribution had normal amylopectin structure and
275 amylose content (Supplemental Figure 2).
276
277 Finally, to confirm that the 6A copy of *MRC* is the only functional homoeolog in tetraploid
278 wheat, we quantified starch granule size distribution in the full set of homozygous genotypes

279 resulting from the crosses that yielded the *mrc-1* and *mrc-2* mutants [indicated as *aa*BB (6A
280 mutant), AA*bb* (6B mutant) and *aabb* (6A and 6B double mutant)]. The size distribution of
281 starch granules was identical between wild type and AA*bb*, and were similarly altered in the
282 *aa*BB and *aabb* genotypes. This provides experimental evidence that the fragment of exon 2
283 on chromosome 6B does not contribute to granule size distribution and is likely to be a
284 pseudogene (Supplemental Figure 3).
285
286 Overall, these data suggest that MRC is required for the normal size distribution of starch
287 granules in wheat endosperm. In tetraploid wheat, mutants in the 6A copy of *MRC*
288 consistently had a higher relative volume of B-type granules in the endosperm than the wild
289 type, and smaller A-type granules. This change in granule size distribution occurred without
290 accompanying changes in total starch content, starch granule shape, amylose content or
291 amylopectin structure.
292
293 *Loss of MRC results in the early initiation of B-type granules*
294 To understand how MRC affects the size distribution of endosperm starch granules, and its
295 effect on A-type or B-type granules specifically, we investigated granule initiation during
296 grain development in the strongest *mrc* mutant, *mrc-1*. We dissected the endosperm of
297 developing grains harvested 8, 14, 20 and 30 days post anthesis (dpa), and measured both the
298 total starch content and number of starch granules. The total starch content of the endosperm
299 increased between each time point, and there was no significant difference between the
300 mutant and the wild type at any time point (Figure 7A). We then quantified the total number
301 of starch granules in the endosperm using a Coulter counter. At the 8 dpa timepoint, the
302 mutant and the wild type contained a similar number of starch granules. Interestingly, for the
303 two subsequent time points (14 dpa and 20 dpa), the mutant endosperms contained almost
304 double the number of starch granules of the wild type, despite similar starch contents (Figure
305 7B). The largest increase in granule number during grain filling was observed between the 20
306 and 30 dpa timepoints in the wild type, and between the 14 and 20 dpa timepoints in the
307 mutant. At the 30 dpa timepoint, the difference in granule number between the mutant and
308 the wild type decreased. Interestingly, we also noted that in both the wild type and mutant,
309 the number of starch granules decreased between the 8 and 14 dpa timepoints. The reason for
310 this is unknown, but it has also been observed in *Aegilops* species – which are close relatives
311 of wheat (Howard et al., 2011).
312

313 We used both a Coulter counter and scanning electron microscopy (SEM) to examine A- to
314 B-type granule ratio in the endosperm throughout grain development. In the wild type, starch
315 granules formed unimodal size distributions at the 8 and 14 dpa timepoints, and only A-type
316 granules with their characteristic flattened morphology were observed using SEM (Figure 8).
317 The A-type granules grew substantially in size between the two timepoints, seen as a shift in
318 the granule size distribution peak. B-type granules only became prominent at the 20 dpa
319 timepoint in the wild type but were already present at 14 dpa in the *mrc-1* mutant, which
320 could be seen as a distinct shoulder that appeared in the granule size distribution of *mrc-1* at
321 14 dpa. Interestingly, the A-type granules in the mutant were the same size as those of the
322 wild type at 8 dpa, but as grain development progressed the *mrc-1* A-type granules were
323 smaller compared to the WT as they grew relatively less in size, particularly as B-type
324 granules were initiated. Taken together, these data suggest that the increased number of
325 granules observed between 14-20 dpa in the *mrc-1* endosperm compared to the WT (observed
326 in Figure 7B) is due to the early initiation of B-type granules in the mutant. The A-type
327 granules in the mutant likely end up smaller than in the WT as the early B-type granules
328 compete with the A-type granules for the substrates of starch synthesis.
329
330 B-type granules typically initiate in close proximity – appearing as 'clusters' in between the
331 A-type granules – and at least some B-type granules form in amyloplast stromules (Parker,
332 1985; Langeveld et al., 2000). Given the unusual timing of B-type granule initiation in *mrc-1*,
333 we explored whether the loss of MRC also affected the location of B-type granule initiation.
334 First, we harvested grains during their development (10, 15, and 20 dpa), subjected them to
335 critical point drying, and imaged sections through the endosperm tissue using SEM.
336 Consistent with the findings from the purified starch granules, B-type granules were
337 prominent already at 10 dpa in the mutant, whereas they only became prominent after 20 dpa
338 in the wild type (Figure 9A). The B-type granules occurred in clusters in the mutant that
339 resembled those of the wild type. Secondly, we examined sections from developing grain
340 tissue (15 dpa) using light and electron microscopy. For light microscopy, sections were
341 stained with toluidine blue (a negative stain for starch). At 15 dpa, most starch granules in the
342 wild-type endosperm were flattened A-type granules, and there were very few B-type
343 granules visible (Figure 9B). However, in the endosperm of the *mrc-1* mutant, many clusters
344 of B-type granules were present. Thus, we used transmission electron microscopy (TEM) to
345 investigate whether the multiple B-type granules in *mrc-1* occurred within single amyloplasts,
346 particularly in stromules. Indeed, multiple B-type granules were enclosed within amyloplasts,

347 and the elongated morphology of these amyloplast regions strongly suggested that they are
348 stromules (Figure 9C). It is difficult to determine the exact percentage of B-type granules in
349 stromules relative to those that are not, as stromules are difficult to observe in two-
350 dimensional electron microscopy sections. However, aside from their earlier occurrence in
351 the mutant, we did not observe anything unusual about the location of B-type granules in the
352 *mrc-1* mutant.
353
354 In conclusion, B-type granule initiation during wheat grain development is under both spatial
355 and temporal control, and MRC appears to be required for this temporal control. It is
356 expressed during early grain development, and loss of MRC leads to the early initiation of B-
357 type granules. We therefore propose that MRC acts as a repressor of B-type granule
358 formation in the developing wheat endosperm during early grain development.
359
360 *TaMRC promotes granule initiation in wheat leaves*
361 Considering the role of MRC in promoting granule initiation in Arabidopsis leaves (Seung et
362 al., 2018; Vandromme et al., 2019), it was surprising that MRC repressed B-type granule
363 formation in wheat endosperm. We therefore investigated whether this repressive role also
364 applies to granule initiation in wheat leaves, which would suggest a divergence in MRC
365 function in wheat compared to Arabidopsis; or whether there was a tissue-level divergence in
366 MRC function in wheat, where MRC promotes granule initiation in wheat leaves as it does in
367 Arabidopsis leaves.
368
369 To assess granule number, shape and size in leaf chloroplasts of our wheat mutants, leaf
370 tissue was harvested from the middle of the older of two leaves of 10-day-old wheat
371 seedlings and sections were imaged with light microscopy (Figure 10A, B). The number of
372 granules per chloroplast was quantified from these images. We measured three individual
373 plants per genotype for each experiment and compared the mean granules per chloroplast
374 between genotypes using a negative binomial mixed effects model with individual biological
375 replicates as random effect. We first compared all three *mrc* mutants with the WT (Figure
376 10C, Table 1). This showed that *mrc-1* and *mrc-2* had fewer granules per chloroplast than the
377 WT, and like in the endosperm, the *mrc-1* mutant showed the strongest effect, having almost
378 50% fewer granules per chloroplast compared to the wild-type (Table 1). Interestingly, there
379 was no effect observed for *mrc-3*, suggesting that the L289F mutation does not affect MRC
380 function in leaves. We also compared the backcrossed *mrc-1* mutant (*mrc-1* BC2 *aabb*) to the

381 WT and the wild-type segregant (*mrc-1* BC2 AABB) (Figure 10 D, Table 1). The
382 backcrossed line also had fewer granules per chloroplast compared to WT, similar to the non-
383 backcrossed *mrc-1*. However, the wild-type segregant also had significantly fewer granules
384 per chloroplast compared to WT, although not to the same extent as the backcrossed *mrc-1*.
385 Likely due to this difference between the WT and the wild-type segregant, the comparison
386 between the backcrossed *mrc-1* and the wild-type segregant did not come out as significant
387 (Table 1), despite the clear shift in granule number distribution between the two genotypes.
388 Overall, the fewer granules in *mrc* chloroplasts in comparison to wild type suggests that
389 MRC promotes granule initiation in wheat leaves, pointing to distinct roles of MRC across
390 organs.
391
392 While the effect of the *mrc-1* mutation on starch granule number per chloroplast was
393 consistent, two other aspects of leaf starch – granule size and total starch content – appeared
394 to be interdependent and varied between our experiments. We quantified the size of granules
395 from these images by measuring the area of granules in the sections. The distributions
396 showed a trend towards larger granule sizes in the *mrc-1* mutant (Figure 10E, F). However,
397 after fitting a linear mixed effects model with individual biological replicates as random
398 effect (Table 2), pairwise comparisons showed no differences between any of the non-
399 backcrossed *mrc* mutants and wild type. However, in the experiment comparing the
400 backcrossed *mrc-1* mutants to wild type and wild-type segregant, the granules were larger in
401 both backcrossed and non-backcrossed *mrc-1* mutants. Aside from the differences in size,
402 there was no visible difference in starch granule shape in any of the mutants compared to
403 wild type.
404
405 Similar variability between experiments was seen in total starch content, which was measured
406 in both leaves of 10-day-old wheat seedlings at the end of the day, when maximum starch is
407 expected. Our first three experiments compared the genotypes WT, *mrc-1, mrc-2* and *mrc-3*
408 (Experiments 1, 2, 3; Supplemental Table 4), and the pooled data showed a lower starch
409 content in all *mrc* mutants compared to wild type (Figure 11A). Our next two experiments
410 (Experiments 4 and 5, Supplemental Table 4) compared end of day starch content in WT,
411 *mrc-1, mrc-1* BC2 *aabb* and *mrc-1* BC2 AABB. By contrast, these experiments showed no
412 difference in starch content between *mrc-1* and WT (Figure 11B). In fact, when comparing
413 *mrc1* BC2 *aabb* with *mrc-1* BC2 AABB or with the WT, there was a small increase in starch
414 content in the backcrossed mutant. The reason for the discrepancy between the results from

experiments 1 – 3 compared to experiments 4 and 5 is unknown, but it may indicate that total starch content in wheat leaves is particularly variable and dependent on many environmental and physiological factors.

Most interestingly, lower starch content in *mrc* mutants compared to the wild type was observed in the same batch of plants where we did not observe a significant difference in -granule size between *mrc* mutants (Experiment 2, Figure 10E), and there was identical (or greater) starch content observed for *mrc-1* mutants in the same batch of plants where we observed larger granules for these mutants (Experiment 5, Figure 10F). Since the reduction in granule number described above was consistently observed in all experiments, it is plausible that the effect on granule size depends on starch content, such that the *mrc-1* mutant only produces larger granules under conditions where total starch content is equal. Pooled data from plants harvested at the end of the night (quantified in experiments 1 and 2) showed very low starch content in all three *mrc* mutants, indicating substantial nocturnal starch turnover in all genotypes, and no differences between wild type and mutants (Figure 11C).

Discussion

A novel role for MRC in repressing B-type granule initiation during endosperm starch synthesis

Starch granule initiation remains the most enigmatic part of the starch synthesis process, where we understand little about how the diverse numbers and morphologies of starch granules are determined in our most important crops (Seung and Smith, 2019; Abt and Zeeman, 2020; Chen et al., 2021). Although we know that the initiation of A-type and B-type granules in wheat is spatially and temporally separated, we do not fully understand which proteins are involved in determining these different patterns.

Here, we have demonstrated a novel role of MRC in ensuring the correct timing of B-type granule formation in the wheat endosperm, by repressing B-type granule initiation during early grain development. MRC is expressed in the endosperm between 6–10 dpa but decreases rapidly in expression between 10–15 dpa, remaining low after 15 dpa (Figure 2). This decline in expression coincides with when B-type granules start to form in the wild type (between 14 –20 dpa; Figures 7 - 9). In the *mrc-1* mutant, B-type granules were initiated earlier than in the wild type, already at 10 dpa (Figures 8 and 9), which could be due to the

448 loss of B-type granule repression by MRC in early grain development. There was an
449 increased number of starch granules in the *mrc-1* mutant compared to wild type from 14 to 30
450 dpa (Figure 7), and this increase remained apparent in the mature grains of the backcrossed
451 *mrc-1* mutant (Figure 4).
452
453 We propose that the early initiation of B-type granules results in drastically altered starch
454 granule size distributions in the endosperm. The early appearance of B-type granules in the
455 *mrc-1* mutant means that they compete with A-type granules for substrates for granule
456 growth (i.e., ADP-glucose) from an earlier stage of grain development than in the wild type,
457 resulting in a higher volume of B-type granules and lower volume of A-type granules in the
458 mature mutant grains (Figure 5). At 8 dpa, before the appearance of B-type granules, the size
459 distribution curves of A-type granules were almost identical between mutant and wild type
460 (Figure 8), and it was only at the later stages of grain development following B-type granule
461 initiation that the A-type granules became smaller in the mutant compared to wild type. The
462 lack of difference in A-type granule number and size at 8 dpa suggests that the *mrc-1*
463 mutation did not affect A-type granule initiation.
464
465 Rather, the early B-type granule initiation alone could result in the increased proportion of B-
466 type granule volume in mature grains, possibly caused by a combination of smaller A-type
467 granules and larger and perhaps relatively more numerous B-type granules (Figure 12). We
468 measured a decrease in A-type granule size in all three *mrc* mutants, and an increase in B-
469 type granule size in *mrc-1* and *mrc-2,* but not *mrc-3* (Figure 5). We also observed a slight
470 increase in total granule number in our *mrc-2* and backcrossed *mrc-1* lines (Figure 4B),
471 which may indicate an increase in the number of B-type granules that could also contribute to
472 the higher relative volume of B-type granules in these lines; although it should be noted that
473 there is currently no method for specifically quantifying the number of B-type granules,
474 considering our definition of B-type granules comes from curve fitting volume/size
475 distribution graphs from the Coulter counter. For *mrc-3,* a higher B-type granule volume
476 percentage was observed (Figure 5B) without a measurable increase in B-type granule size or
477 in total granule number (Figure 4B), but it is still possible that there is a relative increase in
478 B-type granule number in *mrc-3*. Small differences in B-type granule number may be
479 difficult to detect as the B-type granules already make up a much larger proportion of the
480 total granule number in wild type.
481

482 Despite all three *mrc* mutants having an increased proportion of B-type granule volume, they
483 differed in severity (Figure 5). The strongest effect on B-type granule percentage was seen in
484 *mrc-1*, and since the phenotypes of the *mrc-1* backcrossed and non-backcrossed lines were
485 similar, the severity of this line is not due to background mutations. The *mrc-1* line may have
486 the strongest phenotype because the premature stop codon occurs earlier in the coding
487 sequence than in *mrc-2*, and it is possible that the truncated protein in *mrc-2* is partially
488 functional. The *mrc-3* mutant had the weakest phenotypes, suggesting the Leu289Phe
489 mutation might also produce a partially functional protein.
490
491 However, the phenotype of the wild-type segregant from the *mrc-1* backcross was not
492 identical to the wild type, indicating the presence of additional background mutations in the
493 wild-type segregant line. This line had slightly higher TGW and grain size, decreased grains
494 per plant (Figure 3), and a small increase in B-type granule volume percentage (Figure 5)
495 compared to the wild type. The presence of background mutations is not unusual in these
496 EMS-mutagenised wheat TILLING lines (Uauy et al., 2017), and importantly, the effects
497 observed in the wild-type segregant were minor compared to the effects observed in the
498 mutants.
499
500 *MRC has tissue-specific roles in promoting or repressing granule initiation*
501 Since wheat produces starch in both leaves and endosperm, the effects of *mrc* mutations
502 could be explored in both organs. We discovered that MRC has contrasting functions in the
503 endosperm compared to the leaves. Rather than repressing granule initiation, MRC promotes
504 granule initiation in the leaves, similar as in Arabidopsis leaves, although the mutant
505 phenotype in wheat appears to be less severe than in Arabidopsis. In Arabidopsis *mrc*
506 mutants, there is one large granule per chloroplast rather than the multiple smaller granules in
507 wild-type chloroplasts (Seung et al., 2018; Vandromme et al., 2019). By contrast, the wheat
508 *mrc* chloroplasts still have multiple, but fewer granules per chloroplast (Figure 10). This
509 difference in phenotype severity is similar to those observed for the orthologs of other
510 granule initiation proteins of Arabidopsis (BGC1 and SS4) in wheat (Hawkins et al., 2021;
511 Watson-Lazowski et al., 2022). The *mrc-1* and *mrc-2* mutants both have fewer granules per
512 chloroplast compared to wild type, with *mrc-1* having the strongest effect, consistent with the
513 endosperm phenotype. Also similar to the endosperm phenotype, the wild-type segregant
514 shows slightly fewer granules per chloroplast compared to wild type, indicating the
515 background mutations also have an effect in the leaves.

516

517 The primary effect of the *mrc* mutations in leaves was the reduction in granule number per
518 chloroplast, but we also saw varying effects on granule size. In one set of experiments, we
519 detected larger granules in *mrc-1* compared to wild type, although in another set we did not
520 (Figure 10). This appears to be linked to whether a change in total leaf starch content was
521 observed or not, since in both experiments, there was a reduced number of starch granules in
522 the mutants. In the experiment where there was no difference in total starch at the end of the
523 day, the individual (fewer) granules were larger in the mutant, as would be expected.
524 However, in the experiment where the total starch content was lower in the *mrc-1* mutant
525 compared to wild type, the increase in granule size was not observed.
526

527 In Arabidopsis, lack of MRC does not reduce the total end of day leaf starch content; in fact,
528 this is slightly higher in the mutant compared to the wild type (Seung et al., 2018). Overall, in
529 wheat leaves the effect of *mrc* mutations on the total end of day starch content was variable in
530 our experiments (Figure 11). We used both leaves of 10-day old seedlings rather than older
531 plants to minimise the variability in starch content across leaves which we observed in mature
532 plants, but this did not prevent the variability across experiments, perhaps suggesting that
533 starch content in wheat leaves may be more sensitive to small differences in environmental
534 conditions. This could reflect differences in the regulation of starch turnover in wheat vs.
535 Arabidopsis leaves, since soluble sugars make up the majority of the wheat leaf carbohydrate
536 content and are thought to be more important as a storage reserve than starch (Nie et al.,
537 1995; Müller et al., 2018; Watson-Lazowski et al., 2022). These differences may also
538 contribute to the less severe effect on granule number in wheat *mrc* mutants compared to
539 Arabidopsis leaves. The effect of MRC on leaf starch granule initiation is likely to differ
540 depending on the developmental stage, so future studies should focus on the biochemistry of
541 starch granule initiation across leaf and plant development to reveal a complete picture of the
542 role of MRC and other granule initiation proteins in the wheat chloroplast. In Arabidopsis,
543 reduced *At*SS4 abundance has a much stronger effect on granule formation in younger leaves
544 compared to mature leaves (Crumpton-Taylor et al., 2013).
545

546 *Exploring the biochemical basis of the contrasting roles of MRC between organs*
547 Since MRC is a long coiled-coil protein with no known enzymatic domains, it is possible that
548 it can exert opposite effects on granule initiation by interacting with different interaction
549 partners. The Arabidopsis *At*MRC can interact directly with *At*SS4 in yeast two hybrid

550 (Vandromme et al., 2019), and in Arabidopsis leaves *At*MRC was also pulled down in
551 association with *At*PTST2, the ortholog of wheat BGC1 (Seung et al., 2018). Therefore, it is
552 possible that in wheat, protein-protein interactions also play an important role in the function
553 of MRC, although the nature of the interactions may be quite different. Recent work has
554 begun to uncover the distinct roles of Arabidopsis starch granule initiation orthologs in wheat
555 – in the endosperm, SS4 restricts granule initiation during early grain development to ensure
556 proper A-type granule formation and mutants defective in SS4 form compound granules
557 (Hawkins et al., 2021). Similar, but less severe, is the *bgc1* mutant in wheat which also forms
558 irregular compound-like granules but has a higher proportion of normal-looking A-type
559 granules than *ss4* mutants (Chia et al., 2020; Hawkins et al., 2021). BGC1 not only represses
560 granule initiation during A-type granule formation, but also promotes B-type granule
561 formation, as mutants with reduced gene dosage of BGC1 have fewer B-type granules than
562 wild type, with no apparent impact on A-type granules (Chia et al., 2017; Chia et al., 2020).
563
564 However, a B-type granule suppressing mechanism during early grain development, like we
565 report here for MRC, has not previously been described, and suggests that MRC and BGC1
566 might have opposing roles in the wheat endosperm, despite their similar initiation promoting
567 roles seen in leaves of Arabidopsis (Seung et al., 2017; Seung et al., 2018) and wheat
568 (Watson-Lazowski et al., 2022). Similarly, wheat SS4 also promotes leaf granule initiation,
569 as mutants had mostly starchless chloroplasts in the leaves (Hawkins et al., 2021). Together
570 with our finding for MRC, this suggests that there may be more distinct differences for
571 granule initiation proteins between different organs of the same species in comparison to the
572 same organs from different species. The Arabidopsis granule initiation proteins localise to
573 distinct puncta in the chloroplast, but we do not yet know anything about the localisation of
574 these wheat orthologs in the chloroplast or amyloplast. In the future, exploring the protein
575 localisation, protein-protein interactions, and the connection between the two in both tissues
576 could reveal what underpins these distinct functions of MRC.
577
578 The specific effect of the L289F mutation in the *mrc-3* mutant on endosperm starch may
579 provide an important clue in these studies, since *mrc-3* had increased B-type granule
580 percentage in the endosperm, but no differences in granule number in leaves. Determining
581 whether the L289F mutation affects protein conformation, interactions and localisation might
582 help dissect the differences in MRC function in leaves versus endosperm.
583

584 *MRC as a gene target for biotechnological modification of starch granule size*
585 There is significant industrial interest in manipulating starch granule size in crop species, as
586 granule size affects the physico-chemical properties of starch and digestibility (Jobling, 2004;
587 Lindeboom et al., 2004; Chen et al., 2021; Li et al., 2021). Our results establish MRC as a
588 promising gene target for modifying starch granule size distribution in wheat, specifically to
589 achieve smaller starch granules and a narrower granule size distribution range than
590 conventional cultivars. Small granules are more efficiently digested *in vitro* than large
591 granules, due to their larger surface area to volume ratio (Dhital et al., 2010). Possible uses
592 for wheat *mrc* starch within the food industry include pasta making, where more B-type
593 granules positively affect pasta quality due to their higher rate of water absorption (Soh et al.,
594 2006). Wheat *mrc* starch may also be useful in industrial applications like papermaking and
595 biodegradable plastics, where small granules are desirable (Lindeboom et al., 2004).
596 Functional tests can be directly performed on our material to provide proof of concept that
597 the altered granule size distribution in the *mrc* mutants improves grain/starch quality.
598
599 MRC is a promising target because different granule size can be achieved without
600 accompanying effects on overall plant growth (Figure 3), on grain weight and total starch
601 content (Figure 4), starch granule shape (Figure 6), or on amylopectin structure and amylose
602 content (Supplemental figure 3). It is also ideal that the B genome homeolog has become a
603 pseudogene (Figure 1), meaning that only one or two homeologs need to be mutated in durum
604 and bread wheat respectively to achieve an effect on granule size. Further, we have also
605 demonstrated that different mutations in MRC can be used to fine-tune the volume of B-type
606 granules in endosperm starch, such as those in *mrc-2* and *mrc-3* to achieve moderate
607 increases, and *mrc-1* to achieve larger increases. Along this line, we are currently
608 investigating whether overexpression of MRC can be used to reduce the volume of B-type
609 granules.
610
611 Since the repression of B-type granule initiation is likely to be a role specific to Triticeae
612 species carrying a bimodal size distribution of endosperm starch, it remains to be determined
613 what the role of MRC is in cereal species that do not have a bimodal distribution of starch
614 granules, such as those that have compound granules (e.g. in rice). Also, oats have a bimodal
615 distribution of starch granules, with large compound granules and smaller simple granules.
616 However, in oat, the smaller granules initiate at the same time as the larger compound
617 granules (Saccomanno et al., 2017), and it would therefore be interesting to determine if

618 differences in MRC function play a role in timing the initiation of the small granules during
619 oat endosperm development. Exploring the role of MRC in multiple crop species would
620 therefore not only reveal the molecular differences that result in distinct spatiotemporal
621 patterns of granule initiation between species, but also potentially increase its
622 biotechnological potential.
623

624 **Materials and Methods**

625 *TaMRC bioinformatic analysis*

626 To characterize *TtMRC-B1* in tetraploid wheat, we aligned the whole genome-sequencing
627 reads of *Triticum dicoccoides* (n = 10) and *Triticum turgidum ssp. durum* (n = 10) from Zhou
628 et al., 2020 against the 'tetraploid' version of the Ref-Seqv1.0 Chinese Spring assembly
629 (Appels et al., 2018). We used HiSat2-v-2.1.0 (Kim et al., 2019) with the default settings and
630 visualized the read alignments on the genetic signatures of retrotransposon insertion on *MRC-*
631 *B1* (Figure 1B) using Integrated Genomics Viewer (Robinson et al., 2011). Phylogenetic
632 analyses were performed as described in Seung et al., (2018).
633

634 *Plant materials and growth*

635 EMS mutants of tetraploid wheat (*Triticum turgidum* cv. Kronos) carrying mutations in
636 *TtMRC-A1* and the chromosome 6B pseudogene were identified from the wheat *in silico*
637 TILLING database (http://www.wheat-tilling.com; Krasileva et al., 2017) and obtained from
638 the John Innes Centre Germplasm Resource Unit. The selected mutants for *TtMRC-A1* were
639 Kronos3272(K3272), Kronos598(K598) and Kronos4681(K4681); while
640 Kronos4305(K4305) and Kronos3078(K3078) were selected for the 6B pseudogene. From
641 these mutants, we generated three different sets of lines. The *mrc-1* lines descend from a
642 cross between K3272 and K3078, while the *mrc-2* lines descend from a cross between K4681
643 and K4305. For both crosses, *aa*BB, AA*bb* and *aabb* genotypes were obtained in the F2
644 generation. The *mrc-3* lines are the original K598 mutants. The KASP markers used to
645 genotype the mutations are provided in Supplemental Table 3.
646

647 For all experiments on grains, plants were grown in soil in a controlled environment room
648 fitted with fluorescent lamps and supplemented with LED panels. The chambers were set to
649 provide a 16-h light/8-h dark cycle, with light intensity of 300 µmol photons m^{-2} s^{-1} and
650 relative humidity of 60%. Temperature was set to 20°C during the light period, and 16°C

651 during the dark period. Grains were harvested when the entire spike had senesced and dried
652 (approximately 4 months after sowing). The grains from the first three tillers were used for
653 analysis. For experiments on leaves, plants were grown in a controlled environment chamber
654 with the same settings as above. Leaves were harvested 10 days after germination, when two
655 leaves were present. Both leaves were harvested for total starch quantification, and a section
656 from the middle of the older leaf was used for light microscopy.
657
658 *Grain morphometrics*
659 The number of grains harvested per plant, as well as grain size traits (area, thousand grain
660 weight) were quantified using the MARViN seed analyser (Marvitech GmbH, Wittenburg).
661 Multiple grains from each plant (15 - 88 individual grains per plant) were measured for grain
662 area to calculate the average value for each plant, and these values were used in the plots of
663 Figure 3F and the analysis of Supplemental Table 2D.
664
665 *Starch purification from mature grains or developing endosperm*
666 Starch was purified from mature grains using 3-6 grains per extraction. Dry grains were
667 soaked overnight at 4°C in 5 mL of sterile water. The softened grains were homogenised in
668 10 mL sterile water using a mortar and pestle, and the homogenate was filtered through a 100
669 µm mesh. The starch was pelleted by centrifugation at 3,000*g* for 5 minutes, and resuspended
670 in 2 mL of water. The resuspended starch was loaded on top of a 5 mL 90% Percoll (Sigma)
671 cushion buffered with 50 mM Tris-HCl, pH 8, and was spun at 2,500*g* for 15 minutes. We
672 verified that no intact granules were left in the Percoll interface after the spin. The starch
673 pellet was washed twice with wash buffer (50 mM Tris-HCl, pH 6.8; 10 mM EDTA; 4%
674 SDS; and 10 mM DTT), then three times with water, followed by a final wash in absolute
675 ethanol. The starch was then air dried overnight.
676
677 For starch extraction from developing endosperm, developing grains were harvested at the
678 indicated timepoints and were snap frozen in liquid nitrogen and stored at -80°C until
679 analysis. Each grain was thawed just prior to extraction and the endosperm was carefully
680 dissected and placed into a chilled tube and weighed. The tissue was then homogenised in
681 sterile water with a pestle, then filtered through a 60 µm mesh. The pellet was washed three
682 times in 90% Percoll (Sigma) buffered with 50 mM Tris-HCl, pH 8, then three times with
683 wash buffer (as above), followed by three times with water.
684

685 *Coulter counter analysis of starch granule size and number*
686 For profiles of granule size distribution, purified starch was suspended in Isoton II diluent
687 (Beckman Coulter) and analysed with a Multisizer 4e Coulter counter fitted with a 70 µm
688 aperture (Beckman Coulter). Granules were counted either in volumetric mode, measuring 1
689 mL from a total 100 mL volume preparation containing 20 µL of purified starch or set to
690 count at least 100,000 granules. For calculations of granule counts in volumetric mode, the
691 number of granules per mg grain weight was back calculated to the total starting grain
692 weight. The granules were sized, with the Coulter counter collecting the data using
693 logarithmic bins for the granule diameter (standard settings).
694
695 For each plant, to calculate the mean A- and B-type granule size, as well as relative B-type
696 granule volume, we fitted a mixed bimodal gaussian curve to the distribution using R
697 (https://github.com/JIC-CSB/coulter_counter_fitting). As the data collection on the Coulter
698 counter is set to logarithmic bins on the x-axis, for these calculations and for the traces in
699 Figures 5A, 8A, and Supplemental Figure 3, we transformed the x-axis to even bins, by
700 changing the y-axis to volume percentage density (volume percentage for each bin divided by
701 bin width). For each of the extracted phenotypes of mean A- and B-type granule size and
702 relative B-type granule volume, we fitted individual linear models and performed a one-way
703 ANOVA and Tukey post-hoc tests for pairwise comparisons of the genotypes, using the lm()
704 and emmeans() functions in R, from the 'stats' and 'emmeans' packages. Nine individual
705 plants per genotype were used for this experiment.
706
707 *Light and electron microscopy*
708 For light microscopy of starch granules in leaf chloroplasts, leaf material (1.5 mm x 1.5 mm
709 squares) was harvested and fixed in 2.5% glutaraldehyde in 0.05 M sodium cacodylate, pH
710 7.4, which was vacuum infiltrated into the leaf. The segments were post-fixed with osmium,
711 then dehydrated in an ascending ethanol series, and embedded in LR white resin using EM
712 TP embedding machine (Leica). Semi-thin sections (0.5 µm thick) were produced from the
713 embedded leaves using a glass knife and were dried onto PTFE-coated slides. Chloroplasts
714 and cell walls were stained using toluidine blue stain (0.5% toluidine blue 'O', 0.5% sodium
715 borate) for 1 min. Starch was stained using reagents from the Periodic Acid-Schiff staining
716 kit (Abcam): using a 30 min incubation with periodic acid solution, followed by 5 min with
717 Schiff's solution. Then, chloroplasts and cell walls were again stained using toluidine blue

718 stain for 1 min. The sections were mounted with Histomount (National Diagnostics) and
719 imaged on a DM6000 microscope with 63X oil immersion lens (Leica).
720
721 For light microscopy of endosperm sections from mature grains, thin sections (1 µm thick) of
722 mature grains were made using a microtome fitted with a glass knife. Sections were mounted
723 onto a glass slide and stained with 3% Lugol's iodine solution (Sigma) prior to imaging on a
724 DM6000 (Leica) or AxioObserver Z1 (Zeiss) microscope.
725
726 For light/electron microscopy of developing endosperm tissue, developing grains (15 dpa)
727 were harvested into 4% paraformaldehyde, 2.5% glutaraldehyde in 0.05 M sodium
728 cacodylate, pH 7.4. The osmium post-fixation, dehydration and embedding into LR white
729 resin was done as described above for leaves. For light microscopy, semi-thin sections were
730 stained with toluidine blue and imaged as described above.
731
732 For transmission electron microscopy (TEM), ultra-thin sections (approximately 90 nm) were
733 produced from the embedded grains by sectioning with a diamond knife using a Leica UC7
734 ultramicrotome (Leica, Milton Keynes). The sections were picked up on 200 mesh copper
735 grids which had been formvar and carbon coated, then stained with 2% (w/v) uranyl acetate
736 for 1hr and 1% (w/v) lead citrate for 1 minute, washed in distilled water and air dried. The
737 grids were viewed in a FEI Talos 200C transmission electron microscope (FEI UK Ltd,
738 Cambridge, UK) at 200kV and imaged using a Gatan OneView 4K x 4K digital camera
739 (Gatan, Cambridge, UK) to record DM4 files.
740
741 For scanning electron microscopy (SEM): For imaging starch granules, a drop of purified
742 starch suspended in water (5 mg/mL) was air-dried onto a glass coverslip attached onto an
743 SEM stub. For imaging sections through developing endosperm, harvested grains were fixed
744 in 2.5% glutaraldehyde in 0.05 M sodium cacodylate, pH 7.4. The fixative was removed by
745 washing with 0.05 M sodium cacodylate, pH 7.4, after which the grains were dehydrated in
746 an ascending ethanol series, and then subjected to critical point drying in a CPD300
747 instrument (Leica) according to the manufacturer's instructions. Thick transverse sections
748 were produced from the dried grains and were glued onto SEM stubs. All stubs were sputter
749 coated with gold and observed using either a Supra 55 VPFEG (Zeiss) or Nova NanoSEM
750 450 (FEI) SEM instrument.
751

752 *Analysis of leaf light microscopy images*
753 For quantification of the number of granules per chloroplast, light microscopy images from
754 three individual plants of each of experiments 2 and 5 were used (Supplemental Table 4).
755 Using the cell counter plug-in in ImageJ, the number of granules per chloroplast were
756 counted manually, until 200 – 250 chloroplasts were reached. Cells were chosen across the
757 section, where most of the granules were stained well and clearly visible, and cells directly
758 next to vasculature were avoided. It should be noted that these are counts of granule sections,
759 rather than the actual numbers of granules per chloroplast, as the actual number cannot be
760 determined from two-dimensional sections. As much as possible, all chloroplasts in a cell
761 were counted to avoid bias, although occasionally a few chloroplasts where the granules were
762 unclear had to be omitted. Both lighter and darker stained granules were counted, but
763 occasionally light-staining patches that were difficult to discern as granules were observed in
764 all samples, and these were not included in the count.
765
766 For quantification of the granule size, we analysed the same samples as for the granules per
767 chloroplast, using the 'analyse particles' function in ImageJ, and manually adjusted the
768 thresholding in an image until the dark granules in the images were correctly separated. This
769 was done for several images across the section, until 100 – 400 granules were reached for
770 each plant. As much as possible, we removed instances where the thresholding had fused
771 multiple granules in proximity by checking obvious outliers against the original images.
772
773 For the statistics of the quantification of the number of granules per chloroplast, we consulted
774 the Statistical Services Centre Ltd (Reading, UK), who wrote the statistical analysis script in
775 R for us, available at
776 [https://github.com/Jiaawen/2022_MRC_wheat_Rscripts/tree/main/Fig10]. We used a
777 negative binomial mixed effects model, since we were analysing count data and wanted to
778 account for both the random effect of biological replicate and the frequency distribution of
779 number of granules per chloroplast. We used the mixed_model() function with
780 'family=negative.binomial' from the 'GLMMadaptive' package, and the emmeans() function
781 from the 'emmeans' package for pairwise comparisons in R. Our data had overdispersion
782 when fitting a Poisson model but not when using a negative binomial. We used individual
783 plants as the random effect (for both experiments: 3 plants for each of 4 genotypes – 12
784 plants total), and genotype as fixed effect.
785

786 For the statistics of the granule area, we used a linear mixed effects model, also with the
787 individual plants as random effect and genotype as fixed effect. We used the lmer() function
788 from the 'lmerTest' package, and the emmeans() function from the 'emmeans' package for
789 pairwise comparisons.
790
791 *Quantification of starch content in leaves and endosperm*
792 Starch was quantified in leaf tissue as previously described (Smith and Zeeman, 2006).
793 Briefly, frozen leaf tissue was ground into a powder with a ball mill and then extracted with
794 perchloric acid. Starch in the insoluble fraction of the extraction was gelatinised at 95°C and
795 digested to glucose with α-amylase (Megazyme) and amyloglucosidase (Roche). The glucose
796 released was measured using the hexokinase/glucose-6-phosphate dehydrogenase method
797 (Roche). Starch content (in glucose equivalents) was calculated relative to the original dry
798 weight of the analysed grains.
799
800 Five individual experiments were done to quantify the total end of day leaf starch content
801 (Supplemental Table 4). One set of genotypes was measured in experiments 1 – 3: WT, *mrc-*
802 *1, mrc-2, mrc-3.* Another set was measured in experiments 4 and 5: WT, *mrc-1,* the double
803 backcrossed *mrc-1* BC2 *aabb* and the wild-type segregant from that backcross, *mrc-1* BC2
804 AABB. Therefore, in the statistical analysis experiments 1, 2, 3 were pooled together and
805 experiments 4 and 5 were pooled together. An ANOVA using a fixed effects model showed
806 no interaction between the experiment effect and genotype effect, and experiment and
807 genotype were set as fixed effects in our linear model. We fitted individual linear models for
808 end of day starch in experiments 1 – 3, end of day starch in experiments 4 & 5 and end of
809 night starch in experiments 1 & 2. Then we performed ANOVA and Tukey post-hoc tests
810 using these linear models for pairwise comparisons of the genotypes. For the details of
811 number of replicates, see Supplemental Table 4. We used the lm() function from the 'stats'
812 package in R for the linear models, and used the emmeans() function from the 'emmeans'
813 package for calculating adjusted means and pairwise comparisons.
814
815 A similar method to leaves was used for starch quantification in grains. Mature grains (5-6
816 grains) were soaked overnight at 4°C in 5 mL of sterile water and were homogenised using a
817 mortar and pestle. Developing endosperm tissue was extracted in 1 mL of sterile water with
818 the pestle. Insoluble material in an aliquot of the homogenate was collected by centrifugation

819 at 5,000*g* for 5 mins, then washed once in 0.7 M perchloric acid, once in sterile water, then
820 three times in 80% ethanol. The pellet was then resuspended in water. Starch in the pellet was
821 gelatinised by heating at 95°C for 15 min, then digested using α-amylase (Megazyme) and
822 amyloglucosidase (Roche).
823
824 *Analysis of amylopectin structure and amylose content*
825 Amylopectin structure and amylose content were analysed using purified starch. Amylopectin
826 structure in terms of chain length distribution was quantified using High Performance Anion
827 Exchange Chromatography with Pulsed Amperometric Detection (HPAEC-PAD) (Blennow
828 et al., 1998). For amylose content, granules were dispersed in DMSO and quantified using an
829 iodine-binding method (Warren et al., 2016).
830
831 *Statistics*
832 All statistical analyses were done in R version 4. Overall, we used the emmeans() function
833 from the 'emmeans' package throughout for pairwise comparisons. For most experiments, we
834 used linear models using the lm() function from the 'stats' package and did one-way
835 ANOVAs with Tukey post-hoc tests. Details for individual experiments where we used other
836 models with more than a single fixed effect are described above for the relevant sections.
837 Tables 1, 2 and Supplemental Table 2 also describe details of statistics for individual
838 experiments.
839
840 *Accession numbers*
841 The accession numbers corresponding to the genes investigated in this study are*: Tt*MRC-A1
842 (TRITD6Av1G081580), *Ta*MRC-A1 (TraesCS6A02G180500), *Ta*MRC-D1
843 (TraesCS6D02G164600).
844
845
846 **Acknowledgements**
847 The authors thank the John Innes Centre (JIC) Horticultural Services for providing growth
848 facilities and maintenance of plant material, and JIC Bioimaging for providing access to
849 microscopes. This work was funded through a John Innes Foundation (JIF) Chris J. Leaver
850 Fellowship (to D.S), a Biotechnology and Biological Sciences Research Council (BBSRC,
851 UK) Future Leader Fellowship BB/P010814/1 (to D.S.), a JIF Rotation Ph.D. studentship (to

J.C. and Y.C.) and BBSRC Institute Strategic Programme grants BBS/E/J/000PR9790, BBS/E/J/000PR9799 and BB/P016855/1 (to the John Innes Centre).

Author contributions

J.C. and D.S. conceived the study. J.C., Y.C., A.W-L., F.J.W., A.B., C.U., and D.S. designed the research. J.C., Y.C., A.W-L., E.H., J.E.B., B.F., R.D.B., K.C., F.J.W., A.B., C.U., and D.S. performed the research and analysed data; J.C. and D.S. wrote the article with input from all authors.

References

Abt, M.R., and Zeeman, S.C. (2020). Evolutionary innovations in starch metabolism. Current Opinion in Plant Biology **55,** 109-117.

Appels, R., Eversole, K., Stein, N., Feuillet, C., Keller, B., Rogers, J., Pozniak, C.J., Choulet, F., Distelfeld, A., Poland, J., Ronen, G., Sharpe, A.G., Barad, O., Baruch, K., Keeble-Gagnère, G., Mascher, M., Ben-Zvi, G., Josselin, A.-A., Himmelbach, A., Balfourier, F., Gutierrez-Gonzalez, J., Hayden, M., Koh, C., Muehlbauer, G., Pasam, R.K., Paux, E., Rigault, P., Tibbits, J., Tiwari, V., Spannagl, M., Lang, D., Gundlach, H., Haberer, G., Mayer, K.F.X., Ormanbekova, D., Prade, V., Šimková, H., Wicker, T., Swarbreck, D., Rimbert, H., Felder, M., Guilhot, N., Kaithakottil, G., Keilwagen, J., Leroy, P., Lux, T., Twardziok, S., Venturini, L., Juhász, A., Abrouk, M., Fischer, I., Uauy, C., Borrill, P., Ramirez-Gonzalez, R.H., Arnaud, D., Chalabi, S., Chalhoub, B., Cory, A., Datla, R., Davey, M.W., Jacobs, J., Robinson, S.J., Steuernagel, B., van Ex, F., Wulff, B.B.H., Benhamed, M., Bendahmane, A., Concia, L., Latrasse, D., Bartoš, J., Bellec, A., Berges, H., Doležel, J., Frenkel, Z., Gill, B., Korol, A., Letellier, T., Olsen, O.-A., Singh, K., Valárik, M., van der Vossen, E., Vautrin, S., Weining, S., Fahima, T., Glikson, V., Raats, D., Číhalíková, J., Toegelová, H., Vrána, J., Sourdille, P., Darrier, B., Barabaschi, D., Cattivelli, L., Hernandez, P., Galvez, S., Budak, H., Jones, J.D.G., Witek, K., Yu, G., Small, I., Melonek, J., Zhou, R., Belova, T., Kanyuka, K., King, R., Nilsen, K., Walkowiak, S., Cuthbert, R., Knox, R., Wiebe, K., Xiang, D., Rohde, A., Golds, T., Čížková, J., Akpinar, B.A., Biyiklioglu, S., Gao, L., N'Daiye, A., Kubaláková, M., Šafář, J., Alfama, F., Adam-Blondon, A.-F., Flores, R., Guerche, C., Loaec, M., Quesneville, H., Condie, J., Ens, J., Maclachlan, R., Tan, Y., Alberti, A., Aury, J.-M., Barbe, V., Couloux, A., Cruaud, C., Labadie, K., Mangenot, S., Wincker, P., Kaur, G., Luo, M., Sehgal, S., Chhuneja, P., Gupta, O.P., Jindal, S., Kaur, P., Malik, P., Sharma, P., Yadav, B., Singh, N.K., Khurana, J.P., Chaudhary, C., Khurana, P., Kumar, V., Mahato, A., Mathur, S., Sevanthi, A., Sharma, N., Tomar, R.S., Holušová, K., Plíhal, O., Clark, M.D., Heavens, D., Kettleborough, G., Wright, J., Balcárková, B., Hu, Y., Salina, E., Ravin, N., Skryabin, K., Beletsky, A., Kadnikov, V., Mardanov, A., Nesterov, M., Rakitin, A., Sergeeva, E., Handa, H., Kanamori, H., Katagiri, S., Kobayashi, F., Nasuda, S., Tanaka, T., Wu, J., Cattonaro, F., Jiumeng, M., Kugler, K., Pfeifer, M., Sandve, S., Xun, X., Zhan, B., Batley, J., Bayer, P.E., Edwards, D., Hayashi, S., Tulpová, Z., Visendi, P., Cui, L., Du, X., Feng, K., Nie, X., Tong, W., and Wang, L. (2018). Shifting the limits in wheat research and breeding using a fully annotated reference genome. Science **361,** eaar7191.

Bechtel, D.B., Zayas, I., Kaleikau, L., and Pomeranz, Y. (1990). Size-distribution of wheat starch granules during endosperm development. Cereal Chemistry **67,** 59-63.

Blennow, A., Bay-Smidt, A.M., Wischmann, B., Olsen, C.E., and Møller, B.L. (1998). The degree of starch phosphorylation is related to the chain length distribution of the neutral and the phosphorylated chains of amylopectin. Carbohydrate Research **307,** 45-54.

Borrill, P., Ramirez-Gonzalez, R., and Uauy, C. (2016). expVIP: a customizable RNA-seq data analysis and visualization platform. Plant Physiology **170,** 2172-2186.

Chen, J., Hawkins, E., and Seung, D. (2021). Towards targeted starch modification in plants. Current Opinion in Plant Biology **60,** 102013.

Chen, J., Watson-Lazowski, A., Vickers, M., and Seung, D. (2022). Gene expression profile of the developing endosperm in wheat. BioRxiv (link available shortly).

Chia, T., Adamski, N.M., Saccomanno, B., Greenland, A., Nash, A., Uauy, C., and Trafford, K. (2017). Transfer of a starch phenotype from wild wheat to bread wheat by deletion of a locus controlling B-type starch granule content. Journal of Experimental Botany **68,** 5497-5509.

Chia, T., Chirico, M., King, R., Ramirez-Gonzalez, R., Saccomanno, B., Seung, D., Simmonds, J., Trick, M., Uauy, C., Verhoeven, T., and Trafford, K. (2020). A carbohydrate-binding protein, B-GRANULE CONTENT 1, influences starch granule size distribution in a dose-dependent manner in polyploid wheat. Journal of Experimental Botany **71,** 105-115.

Crumpton-Taylor, M., Pike, M., Lu, K.J., Hylton, C.M., Feil, R., Eicke, S., Lunn, J.E., Zeeman, S.C., and Smith, A.M. (2013). Starch synthase 4 is essential for coordination of starch granule formation with chloroplast division during Arabidopsis leaf expansion. New Phytologist **200,** 1064-1075.

Daron, J., Glover, N., Pingault, L., Theil, S., Jamilloux, V., Paux, E., Barbe, V., Mangenot, S., Alberti, A., Wincker, P., Quesneville, H., Feuillet, C., and Choulet, F. (2014). Organization and evolution of transposable elements along the bread wheat chromosome 3B. Genome Biol **15,** 546.

Dhital, S., Shrestha, A.K., and Gidley, M.J. (2010). Relationship between granule size and in vitro digestibility of maize and potato starches. Carbohydrate Polymers **82,** 480-488.

Hawkins, E., Chen, J., Watson-Lazowski, A., Ahn-Jarvis, J., Barclay, J.E., Fahy, B., Hartley, M., Warren, F.J., and Seung, D. (2021). STARCH SYNTHASE 4 is required for normal starch granule initiation in amyloplasts of wheat endosperm. New Phytologist **230,** 2371-2386.

Howard, T., Rejab, N.A., Griffiths, S., Leigh, F., Leverington-Waite, M., Simmonds, J., Uauy, C., and Trafford, K. (2011). Identification of a major QTL controlling the content of B-type starch granules in Aegilops. Journal of Experimental Botany **62,** 2217-2228.

Jobling, S. (2004). Improving starch for food and industrial applications. Current Opinion in Plant Biology **7,** 210-218.

Kim, D., Paggi, J.M., Park, C., Bennett, C., and Salzberg, S.L. (2019). Graph-based genome alignment and genotyping with HISAT2 and HISAT-genotype. Nat Biotechnol **37,** 907-915.

Krasileva, K.V., Vasquez-Gross, H.A., Howell, T., Bailey, P., Paraiso, F., Clissold, L., Simmonds, J., Ramirez-Gonzalez, R.H., Wang, X., Borrill, P., Fosker, C., Ayling, S., Phillips, A.L., Uauy, C., and Dubcovsky, J. (2017). Uncovering hidden variation in polyploid wheat. Proceedings of the National Academy of Sciences **114,** E913-E921.

Langeveld, S.M.J., Van wijk, R., Stuurman, N., Kijne, J.W., and de Pater, S. (2000). B-type granule containing protrusions and interconnections between amyloplasts in developing wheat endosperm revealed by transmission electron microscopy and GFP expression. Journal of Experimental Botany **51,** 1357-1361.

Li, L.F., Zhang, Z.B., Wang, Z.H., Li, N., Sha, Y., Wang, X.F., Ding, N., Li, Y., Zhao, J., Wu, Y., Gong, L., Mafessoni, F., Levy, A.A., and Liu, B. (2022). Genome sequences of five Sitopsis species of Aegilops and the origin of polyploid wheat B subgenome. Mol Plant **15,** 488-503.

Li, M., Daygon, V.D., Solah, V., and Dhital, S. (2021). Starch granule size: Does it matter? Critical Reviews in Food Science and Nutrition **0,** 1-21.

Lindeboom, N., Chang, P.R., and Tyler, R.T. (2004). Analytical, biochemical and physicochemical aspects of starch granule size, with emphasis on small granule starches: a review. Starch - Stärke **56,** 89-99.

Maccaferri, M., Harris, N.S., Twardziok, S.O., Pasam, R.K., Gundlach, H., Spannagl, M., Ormanbekova, D., Lux, T., Prade, V.M., Milner, S.G., Himmelbach, A., Mascher, M., Bagnaresi, P., Faccioli, P., Cozzi, P., Lauria, M., Lazzari, B., Stella, A., Manconi, A., Gnocchi, M., Moscatelli, M., Avni, R., Deek, J., Biyiklioglu, S., Frascaroli, E., Corneti, S., Salvi, S., Sonnante, G., Desiderio, F., Marè, C., Crosatti, C., Mica, E., Özkan, H., Kilian, B., De Vita, P., Marone, D., Joukhadar, R., Mazzucotelli, E., Nigro, D., Gadaleta, A., Chao, S., Faris, J.D., Melo, A.T.O., Pumphrey, M., Pecchioni, N., Milanesi, L., Wiebe, K., Ens, J., MacLachlan, R.P., Clarke, J.M., Sharpe, A.G., Koh, C.S., Liang, K.Y.H., Taylor, G.J., Knox, R., Budak, H., Mastrangelo, A.M., Xu, S.S., Stein, N., Hale, I., Distelfeld, A., Hayden, M.J., Tuberosa, R., Walkowiak, S., Mayer, K.F.X., Ceriotti, A., Pozniak, C.J., and Cattivelli, L. (2019). Durum wheat genome highlights past domestication signatures and future improvement targets. Nature Genetics **51,** 885-895.

Matsushima, R., Yamashita, J., Kariyama, S., Enomoto, T., and Sakamoto, W. (2013). A phylogenetic re-evaluation of morphological variations of starch grains among Poaceae species. Journal of Applied Glycoscience **60,** 131-135.

Müller, L.M., Gol, L., Jeon, J.-S., Weber, A.P.M., Davis, S.J., and von Korff, M. (2018). Temperature but not the circadian clock determines nocturnal carbohydrate availability for growth in cereals. bioRxiv.

Ng, P.C., and Henikoff, S. (2006). Predicting the effects of amino acid substitutions on protein function. Annu Rev Genomics Hum Genet **7,** 61-80.

Nie, G., Hendrix, D.L., Webber, A.N., Kimball, B.A., and Long, S.P. (1995). Increased accumulation of carbohydrates and decreased photosynthetic gene transcript levels in wheat grown at an elevated CO2 concentration in the field. Plant Physiol **108,** 975-983.

Parker, M.L. (1985). The relationship between A-type and B-type starch granules in the developing endosperm of wheat. Journal of Cereal Science **3,** 271-278.

Peng, C., Wang, Y., Liu, F., Ren, Y., Zhou, K., Lv, J., Zheng, M., Zhao, S., Zhang, L., Wang, C., Jiang, L., Zhang, X., Guo, X., Bao, Y., and Wan, J. (2014). FLOURY ENDOSPERM6 encodes a CBM48 domain-containing protein involved in compound granule formation and starch synthesis in rice endosperm. Plant Journal **77,** 917-930.

Ramirez-Gonzalez, R.H., Borrill, P., Lang, D., Harrington, S.A., Brinton, J., Venturini, L., Davey, M., Jacobs, J., van Ex, F., Pasha, A., Khedikar, Y., Robinson, S.J., Cory, A.T., Florio, T., Concia, L., Juery, C., Schoonbeek, H., Steuernagel, B., Xiang, D., Ridout, C.J., Chalhoub, B., Mayer, K.F.X., Benhamed, M., Latrasse, D., Bendahmane, A., International Wheat Genome Sequencing, C., Wulff, B.B.H., Appels, R., Tiwari, V., Datla, R., Choulet, F., Pozniak, C.J., Provart, N.J., Sharpe, A.G., Paux, E., Spannagl, M., Brautigam, A., and Uauy, C. (2018). The transcriptional landscape of polyploid wheat. Science **361**.

Robinson, J.T., Thorvaldsdottir, H., Winckler, W., Guttman, M., Lander, E.S., Getz, G., and Mesirov, J.P. (2011). Integrative genomics viewer. Nat Biotechnol **29,** 24-26.

Roldán, I., Wattebled, F., Mercedes Lucas, M., Delvallé, D., Planchot, V., Jiménez, S., Pérez, R., Ball, S., D'Hulst, C., and Mérida, A. (2007). The phenotype of soluble starch synthase IV defective mutants of Arabidopsis thaliana suggests a novel function of elongation enzymes in the control of starch granule formation. Plant Journal **49,** 492-504.

1011 **Saccomanno, B., Chambers, A.H., Hayes, A., Mackay, I., McWilliam, S.C., and**
1012 **Trafford, K.** (2017). Starch granule morphology in oat endosperm. Journal of Cereal
1013 Science **73,** 46-54.
1014 **Saccomanno, B., Berbezy, P., Findlay, K., Shoesmith, J., Uauy, C., Viallis, B., and**
1015 **Trafford, K.** (2022). Characterization of wheat lacking B-type starch granules.
1016 Journal of Cereal Science **104**.
1017 **Saito, M., Tanaka, T., Sato, K., Vrinten, P., and Nakamura, T.** (2017). A single
1018 nucleotide polymorphism in the "Fra" gene results in fractured starch granules in
1019 barley. Theoretical and Applied Genetics **131,** 353-364.
1020 **Seung, D.** (2020). Amylose in starch: towards an understanding of biosynthesis, structure and
1021 function. New Phytologist **228,** 1490-1504.
1022 **Seung, D., and Smith, A.M.** (2019). Starch granule initiation and morphogenesis – progress
1023 in Arabidopsis and cereals. Journal of Experimental Botany **70,** 771-784.
1024 **Seung, D., Schreier, T.B., Bürgy, L., Eicke, S., and Zeeman, S.C.** (2018). Two plastidial
1025 coiled-coil proteins are essential for normal starch granule initiation in Arabidopsis.
1026 Plant Cell **30,** 1523-1542.
1027 **Seung, D., Boudet, J., Monroe, J.D., Schreier, T.B., David, L.C., Abt, M., Lu, K.-J.,**
1028 **Zanella, M., and Zeeman, S.C.** (2017). Homologs of PROTEIN TARGETING TO
1029 STARCH control starch granule initiation in Arabidopsis leaves. Plant Cell **29,** 1657-
1030 1677.
1031 **Smith, A.M., and Zeeman, S.C.** (2006). Quantification of starch in plant tissues. Nature
1032 Protocols **1,** 1342-1345.
1033 **Smith, A.M., and Zeeman, S.C.** (2020). Starch: A flexible, adaptable carbon store coupled
1034 to plant growth. Annual Review of Plant Biology **71,** 217-245.
1035 **Soh, H.N., Sissons, M.J., and Turner, M.A.** (2006). Effect of starch granule size
1036 distribution and elevated amylose content on durum dough rheology and spaghetti
1037 cooking quality. Cereal Chemistry **83,** 513-519.
1038 **Tetlow, I., and Emes, M.** (2017). Starch biosynthesis in the developing endosperms of
1039 grasses and cereals. Agronomy **7,** 81.
1040 **Uauy, C., Wulff, B.B.H., and Dubcovsky, J.** (2017). Combining traditional mutagenesis
1041 with new high-throughput sequencing and genome editing to reveal hidden variation
1042 in polyploid wheat. Annu Rev Genet **51,** 435-454.
1043 **Vandromme, C., Spriet, C., Dauvillée, D., Courseaux, A., Putaux, J.-l., Wychowski, A.,**
1044 **Krzewinski, F., Facon, M., D'Hulst, C., and Wattebled, F.** (2019). PII1: a protein
1045 involved in starch initiation that determines granule number and size in Arabidopsis
1046 chloroplast. New Phytologist **221,** 356-370.
1047 **Walkowiak, S., Gao, L., Monat, C., Haberer, G., Kassa, M.T., Brinton, J., Ramirez-**
1048 **Gonzalez, R.H., Kolodziej, M.C., Delorean, E., Thambugala, D., Klymiuk, V.,**
1049 **Byrns, B., Gundlach, H., Bandi, V., Siri, J.N., Nilsen, K., Aquino, C.,**
1050 **Himmelbach, A., Copetti, D., Ban, T., Venturini, L., Bevan, M., Clavijo, B., Koo,**
1051 **D.H., Ens, J., Wiebe, K., N'Diaye, A., Fritz, A.K., Gutwin, C., Fiebig, A., Fosker,**
1052 **C., Fu, B.X., Accinelli, G.G., Gardner, K.A., Fradgley, N., Gutierrez-Gonzalez,**
1053 **J., Halstead-Nussloch, G., Hatakeyama, M., Koh, C.S., Deek, J., Costamagna,**
1054 **A.C., Fobert, P., Heavens, D., Kanamori, H., Kawaura, K., Kobayashi, F.,**
1055 **Krasileva, K., Kuo, T., McKenzie, N., Murata, K., Nabeka, Y., Paape, T.,**
1056 **Padmarasu, S., Percival-Alwyn, L., Kagale, S., Scholz, U., Sese, J., Juliana, P.,**
1057 **Singh, R., Shimizu-Inatsugi, R., Swarbreck, D., Cockram, J., Budak, H.,**
1058 **Tameshige, T., Tanaka, T., Tsuji, H., Wright, J., Wu, J., Steuernagel, B., Small,**
1059 **I., Cloutier, S., Keeble-Gagnere, G., Muehlbauer, G., Tibbets, J., Nasuda, S.,**
1060 **Melonek, J., Hucl, P.J., Sharpe, A.G., Clark, M., Legg, E., Bharti, A., Langridge,**

P., Hall, A., Uauy, C., Mascher, M., Krattinger, S.G., Handa, H., Shimizu, K.K., Distelfeld, A., Chalmers, K., Keller, B., Mayer, K.F.X., Poland, J., Stein, N., McCartney, C.A., Spannagl, M., Wicker, T., and Pozniak, C.J. (2020). Multiple wheat genomes reveal global variation in modern breeding. Nature **588,** 277-283.

Warren, F.J., Gidley, M.J., and Flanagan, B.M. (2016). Infrared spectroscopy as a tool to characterise starch ordered structure - A joint FTIR-ATR, NMR, XRD and DSC study. Carbohydrate Polymers **139,** 35-42.

Watson-Lazowski, A., Raven, E., Feike, D., Hill, L., Elaine Barclay, J., Smith, A.M., and Seung, D. (2022). Loss of PROTEIN TARGETING TO STARCH 2 has variable effects on starch synthesis across organs and species. J Exp Bot.

Zhou, Y., Zhao, X., Li, Y., Xu, J., Bi, A., Kang, L., Xu, D., Chen, H., Wang, Y., Wang, Y.-g., Liu, S., Jiao, C., Lu, H., Wang, J., Yin, C., Jiao, Y., and Lu, F. (2020). Triticum population sequencing provides insights into wheat adaptation. Nat Genet **52,** 1412-1422.

Tables

Table 1. Statistics of pairwise comparisons of leaf granule per chloroplast in young wheat leaves, from negative binomial mixed effect models with biological replicate (3 of each genotype) as random effect, using Tukey post-hoc tests. Individual models for each experiment were used. SE = standard error, 95% CI = 95% confidence interval.

contrast	Experiment	ratio	SE	- 95% CI	+ 95 CI	z.ratio	p.value
WT / *mrc-1*	2	1.997	0.190	1.564	2.550	7.271	2.17E-12
WT / *mrc-2*	2	1.390	0.131	1.091	1.769	3.497	0.00265
WT / mrc-3	2	1.091	0.102	0.858	1.387	0.929	0.789273
mrc-1 / mrc-2	2	0.696	0.067	0.544	0.890	-3.783	0.000892
mrc-1 / mrc-3	2	0.546	0.052	0.427	0.698	-6.336	1.41E-09
mrc-2 / mrc-3	2	0.785	0.074	0.616	1.000	-2.564	0.05063
mrc-1* BC2 *aabb* / *mrc-1	5	1.030	0.097	0.810	1.311	0.318	0.988897
mrc-1* BC2 *AABB / mrc-1	5	1.234	0.115	0.971	1.569	2.256	0.108551
mrc-1* BC2 *AABB* / *mrc-1* BC2 *aabb	5	1.198	0.111	0.943	1.522	1.943	0.210022
WT / *mrc-1*	5	1.635	0.152	1.287	2.077	5.285	7.52E-07
WT / *mrc-1* BC2 *aabb*	5	1.587	0.147	1.251	2.014	4.982	3.76E-06
WT / *mrc-1* BC2 *AABB*	5	1.325	0.122	1.045	1.679	3.048	0.012347

Table 2. Statistics of pairwise comparisons of granule size in young wheat leaves, from linear mixed effect models with biological replicate (3 of each genotype) as random effect, using Tukey post-hoc tests and Satterthwaite degrees of freedom calculation. Individual models for each experiment were used. SE = standard error, df = degrees of freedom, 95% CI = 95% confidence interval.

contrast	Experiment	difference	SE	- 95% CI	+ 95 CI	df	t.ratio	p.value
WT – *mrc-1*	2	-0.304	0.125	-0.706	0.0975	7.998	-2.42484	0.149207
WT – *mrc-2*	2	-0.087	0.125	-0.488	0.3150	7.979	-0.69054	0.89788
WT – *mrc-3*	2	0.045	0.125	-0.357	0.4461	7.941	0.356537	0.983352
mrc-2 – mrc-1	2	-0.218	0.126	-0.619	0.1841	8.055	-1.73159	0.368589
mrc-3 – mrc-1	2	-0.349	0.125	-0.750	0.0529	8.017	-2.77906	0.090736
mrc-3 – mrc-2	2	-0.131	0.125	-0.533	0.2704	7.998	-1.04602	0.729078
mrc-1* BC2 *aabb - mrc-1	5	-0.034	0.0394	-0.160	0.0924	7.990	-0.85905	0.825337
mrc-1* BC2 *AABB - mrc-1	5	-0.255	0.0398	-0.381	-0.1289	8.317	-6.41375	0.000799
mrc-1* BC2 *AABB - mrc-1* BC2 *aabb	5	-0.221	0.0400	-0.348	-0.0949	8.470	-5.5362	0.002041
WT - *mrc-1*	5	-0.260	0.0396	-0.386	-0.1335	8.122	-6.56687	0.000748
WT - *mrc-1* BC2 *aabb*	5	-0.226	0.0397	-0.352	-0.0996	8.274	-5.68343	0.001851
WT - *mrc-1* BC2 *AABB*	5	-0.005	0.0401	-0.131	0.1218	8.607	-0.11473	0.999416

Figure Legends

Figure 1. *MRC* homeologs in wheat are encoded on chromosomes 6A and 6D, with a disruption of the 6B homeolog. A) Location of *TaMRC* homeologs on chromosome 6A and 6D. The pink boxes represent *TaMRC* homeologs, while homeologs of the adjacent genes are shown in green (cytochrome P450 family protein), purple (respiratory burst oxidase homolog) and blue (uncharacterised protein). Arrowheads on the boxes indicate direction of transcription. The syntenic region on chromosome 6B has a large insertion, depicted with a black arrowhead. The diagram is drawn to scale, and chromosome coordinates of the region are indicated. **B)** Gene models of the *TaMRC-A1* and *–D1* homeologs and 6B pseudogene. Exons are represented with pink boxes, while light pink boxes represent the 5' and 3' UTRs. On the 6B region, areas with sequence similarity to exon 2 and UTRs of *TaMRC-A1* are indicated, as well as the location of *gypsy* retrotransposons. The locations of the mutations in the *mrc* mutants are depicted with red arrows, and the mutated codons/amino acids are shown in red letters. Large black arrowheads show where the sequence has been truncated for illustration - the length of truncated sequence is indicated above. **C)** Summary of species analysed for the loss of *MRC-B1* during wheat hybridisation

Figure 2. *MRC* is expressed in wheat leaves and wheat endosperm during early grain development. A) Expression of *TaMRC* homeologs between between different tissue types in *Triticum aestivum*. Data were obtained from the wheat expression browser, and values represent transcript per million (TPM) ± SEM from n = 89 (roots), 48 (leaves/shoots), 280 (spike), 166 (grain) samples from different experiments. **B)** Expression of *TtMRC-A1* (TRITD6Av1G081580.1) in the starchy endosperm during grain development of *Triticum turgidum* (variety Kronos). Data are from an RNAseq experiment described in Chen *et al.* (2022). Values represent TPM ± SEM from n = 3 for all timepoints.

Figure 3. Mutations in *MRC* do not affect plant growth or the number and size of grains. A) Photographs of 7-week-old wild type (WT) and *mrc* mutant plants. Bar = 9 cm. **B)** Number of tillers per plant. **C)** Number of grains per plant. **D)** Photographs of mature grains. Bar = 1 cm. **E)** Thousand Grain Weight (TGW) of mature grains. **F)** Grain size, measured as the average area of individual mature grains from each plant. For statistical analysis of B, C, E, F, see Supplemental Table 1. For all boxplots, each box encloses the middle 50% of the distribution, the middle line is the median and the whiskers are the minimum and maximum values within 1.5 of the interquartile range. Dots are measurements from individual plants, with the same group of plants measured for all phenotypes and n = 9 – 10 individual plants.

Figure 4. Mutations in *MRC* have variable effects on total starch in mature grains. A) Total endosperm starch content in mature grains in WT and *mrc* mutants. B) Number of starch granules per mg of grain, counted with a Coulter counter. For A and B, dots on the boxplots indicate individual plants, with n = 8 - 9. Each box encloses the middle 50% of the distribution, the middle line is the median and the whiskers are the minimum and maximum values within 1.5 of the interquartile range. All statistical analyses were performed using a linear model, with a one-way ANOVA and Tukey post-hoc test. Panels on the right indicate differences in means between genotypes from pairwise comparisons based on these models. The difference in means is indicated by a dot, with whiskers showing the 95% confidence interval (CI) of this difference, with the corresponding p-value. Grey indicates the WT or *mrc-1* mutant compared to the backcrossed line with the equivalent genotype at the *MRC* loci, and blue indicates all other pairwise comparisons.

1138 **Figure 5. Endosperm starch in mature grains of *mrc* mutants have altered granule size**
1139 **distribution. A)** Coulter counter traces with evenly binned x-axes show a bimodal
1140 distribution of granule sizes from purified wheat endosperm starch. Data points are mean
1141 values from 9 individual plants of each genotype (3 grains from each plant), with the standard
1142 error of the mean shown as a shaded ribbon. WT and *mrc-1* in the left and right panel are the
1143 same data. **B, C, D)** Mean B-type granule percentage volume (B), A-type granule diameter
1144 (C) and B-type granule diameter (D) values extracted from bimodal log-normal distribution
1145 curves fitted to Coulter counter traces of individual plants. Extracted values and boxplots are
1146 shown on the left, where dots indicate mean values from individual plants (n = 9). Each box
1147 encloses the middle 50% of the distribution, the middle line is the median and the whiskers
1148 are the minimum and maximum values within 1.5 of the interquartile range. All statistical
1149 analyses were performed using linear models for each panel, with a one-way ANOVA and
1150 Tukey post-hoc test. Panels on the right indicate differences in means between genotypes
1151 from pairwise comparisons based on these models. The difference in means is indicated by a
1152 dot, with whiskers showing the 95% confidence interval (CI) of this difference, with the
1153 corresponding p-value. Grey indicates the WT or *mrc-1* mutant compared to the backcrossed
1154 line with the equivalent genotype at the *MRC* loci, and blue indicates all other pairwise
1155 comparisons.
1156
1157 **Figure 6. Endosperm starch granules of mature grains in three wheat *mrc* mutants are**
1158 **similar in shape compared to wild type. A)** Thin sections of mature endosperm tissue were
1159 stained with Lugol's solution and imaged using light microscopy. Bar = 40 µm. **B)** Purified
1160 endosperm starch granules were observed using scanning electron microscopy (SEM). Bar =
1161 20 µm.
1162
1163 **Figure 7. In developing endosperm, granule number increases in *mrc-1* compared to**
1164 **WT despite having similar starch content.** The endosperm was dissected from developing
1165 grains of WT and *mrc-1*, harvested at 8, 14, 20 and 30 dpa, with n = 3 - 4 individual plants
1166 for each genotype per time point, indicated by coloured dots in the upper panels, with the
1167 mean ± 95% confidence interval (CI) in black dots and whiskers. **A)** Starch content of the
1168 endosperm. Values are expressed relative to the fresh weight of the dissected endosperm. **B)**
1169 Starch granule number in the endosperm. Starch was purified from dissected endosperm and
1170 the number of granules was determined using a Coulter counter. Values are expressed relative
1171 to the fresh weight of the dissected endosperm. For A and B, individual linear models were
1172 fitted to the data of each time point, with a one-way ANOVA and Tukey post-hoc test to
1173 compare the means of WT and *mrc-1*. Panels on the bottom summarise the differences in
1174 means from these linear models, indicated by a dot, with whiskers showing the 95% CI of
1175 this difference, with the corresponding p-value.
1176
1177 **Figure 8. The *mrc-1* mutant initiates B-type granules earlier in grain development than**
1178 **in the wild type (WT).** The endosperm was dissected from developing grains of WT and
1179 *mrc-1* harvested at 8, 14, 20 and 30 dpa. **A)** Coulter counter traces with evenly binned x-axes
1180 show the starch granule size distribution of endosperm starch. Distributions are the average of
1181 n = 4 measurements, each carried out on grains harvested from a different plant (three grains
1182 per measurement). Data points are mean values from these 4 measurements, with the standard
1183 error of the mean shown as a shaded ribbon. The B-type granule peak in the *mrc-1* mutant at
1184 14 dpa is indicated with a blue arrow. **B)** Endosperm starch granules were observed using
1185 scanning electron microscopy (SEM). Bars = 20 µm. Examples of A-type granules and B-
1186 type granules are marked with red and blue arrows respectively.

1187 **Figure 9. The early initiating B-type granules in *mrc-1* occur at least partially in**
1188 **stromules. A)** Scanning electron micrographs of developing endosperm tissue subjected to
1189 critical point drying. Grains were harvested from WT and *mrc-1* at 10, 15 and 20 days post
1190 anthesis (dpa). A representative region of each panel has been pseudo-coloured, with A-type
1191 granules in red shading and B-type granules in blue shading. Bars = 50 µm. **B)** Light
1192 micrographs of endosperm sections. Semi-thin sections of embedded developing grains (15
1193 dpa) were stained with toluidine blue as a negative stain for starch granules. Examples of A-
1194 type granules and B-type granules are marked with red and blue arrows respectively. Bars =
1195 50 µm. **C)** Endosperm sections observed using transmission electron microscopy, using the
1196 same samples as in B. The periphery of amyloplast membranes, where visible, are indicated
1197 with a dotted white line. Bars = 1 µm.
1198
1199 **Figure 10. Chloroplasts of *mrc-1* mutants have fewer and larger granules than the wild**
1200 **type. A, B)** Representative light microscopy images of thin sections (500 nm) from the
1201 middle of the older of two leaves in 10-day old wheat seedlings, collected at the end of day.
1202 Sections were stained for starch using periodic acid and Schiff staining. Scale bar = 10 µm.
1203 **C, D)** Distributions of counts of granule sections per chloroplast section, counted from light
1204 microscopy images as in A and B. The three different colours correspond to three individual
1205 plants of each genotype, per experiment. For each sample, 200 – 250 chloroplasts were
1206 counted, with absolute values varying between samples. Dots represent individual
1207 chloroplasts. **E, F)** Distributions of starch granule sizes measured as the area in the light
1208 microscopy images as in A and B. The three different colours correspond to three individual
1209 plants of each genotype, per experiment. 100 – 400 granules were measured in each sample.
1210 Dots represent individual granules. For all boxplots, each box encloses the middle 50% of the
1211 distribution, the middle line is the median and the whiskers are the minimum and maximum
1212 values within 1.5 of the interquartile range. Measurements were made on the same batch of
1213 plants as Figure 11, experiment 2 (panels A, C, E here) and experiment 5 (panels B, D, F
1214 here).
1215
1216 **Figure 11. Loss of MRC has variable effects on the total end of day (ED) leaf starch**
1217 **content in wheat leaves. A)** Pooled starch content data of wheat leaves harvested at the end
1218 of day (ED) in experiments 1 (dark brown, n = 5 – 6 per genotype), 2 (light brown, n = 5 – 6
1219 per genotype) and 3 (orange, n = 16 – 19 per genotype). **B)** Pooled starch content data from
1220 wheat leaves in experiments 4 (dark brown, n = 10 – 15 per genotype) and 5 (light brown, n =
1221 10 – 12 per genotype) harvested at ED. **C)** Pooled starch content data of wheat leaves
1222 harvested at the end of night (EN) in experiments 1 (dark brown, n = 4 – 6 per genotype) and
1223 2 (light brown n = 4 – 6 per genotype) **For all panels**, raw data and boxplots are shown on
1224 the left, where dots indicate values from individual wheat plants, with colours indicating each
1225 experiment. Each box encloses the middle 50% of the distribution, the middle line is the
1226 median and the whiskers are the minimum and maximum values within 1.5 of the
1227 interquartile range. All statistical analyses were performed using a linear model with
1228 genotype and experiment as fixed effects for each panel, ANOVA and Tukey post-hoc tests.
1229 Panels on the right indicate differences in adjusted means of total starch content based on
1230 these models and pairwise comparisons of the genotypes. The difference in means is
1231 indicated by a dot, with whiskers showing the 95% confidence interval (CI) of this difference,
1232 with the corresponding p-value. For A and C, blue indicates comparisons between mutant and
1233 wild type, while grey indicates comparisons between mutants. For B, grey indicates the WT
1234 or *mrc-1* mutant compared to the backcrossed line with the equivalent genotype at the *MRC*
1235 loci, and blue indicates all other pairwise comparisons.

1236 **Figure 12. Model of MRC function in wheat developing endosperm.** MRC is required for
1237 the control of the timing of B-type granule initiation during early grain development. In wild
1238 type, A-type granules initiate around 4 days post anthesis (dpa), and B-type granules initiate
1239 around 15 – 20 dpa. We propose that the expression of MRC during early endosperm
1240 development prevents the B-type granule formation, and B-type granule volume increases as
1241 MRC expression decreases after 10 dpa. This process is disrupted in mutants lacking a
1242 functional MRC protein, and granules initiate already from 10 dpa. The early initiation of B-
1243 type granules provides them with more time and substrate to grow, leading to higher volume
1244 of B-type granules in the mutant at grain maturity compared to the wild type, and a
1245 concomitant decrease in A-type granule size in the mutant.
1246

1247

1248 **Supplemental data**

1249 Supplemental File 1. *Aegilops speltoides* MRC gene model

1250 Supplemental Figure 1. Phylogenetic analysis of wheat MRC sequences.

1251 Supplemental Figure 2. Chain length distribution and amylose content of the *mrc* mutants.

1252 Supplemental Figure 3. The 6B pseudogene does not contribute to granule size distribution

1253 in wheat endosperm starch.

1254 Supplemental Table 1. Reads mapped to retrotransposon insertion genetic signatures on
1255 *MRC-B1.*

1256 Supplemental Table 2. Pairwise comparisons of wheat growth phenotypes.

1257 Supplemental Table 3. KASP markers for genotyping the wheat mutants.

1258 Supplemental Table 4. Summary of leaf starch quantification experiments.

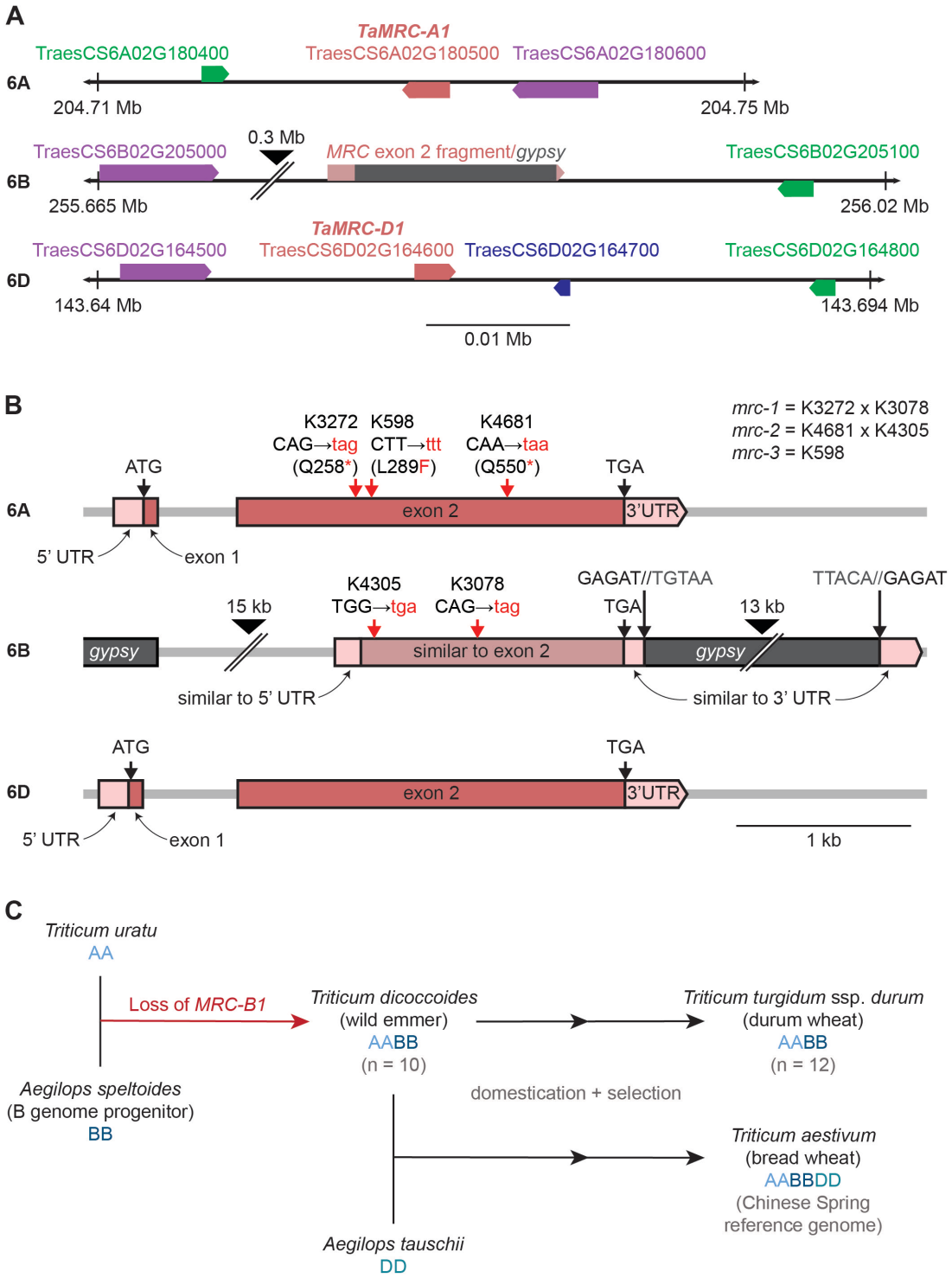

Figure 1. *MRC* homeologs in wheat are encoded on chromosomes 6A and 6D, with a disruption of the 6B homeolog. A) Location of *TaMRC* homeologs on chromosome 6A and 6D. The pink boxes represent *TaMRC* homeologs, while homeologs of the adjacent genes are shown in green (cytochrome P450 family protein), purple (respiratory burst oxidase homolog) and blue (uncharacterised protein). Arrowheads on the boxes indicate direction of transcription. The syntenic region on chromosome 6B has a large insertion, depicted with a black arrowhead. The diagram is drawn to scale, and chromosome coordinates of the region are indicated. **B)** Gene models of the *TaMRC-A1* and *–D1* homeologs and 6B pseudogene. Exons are represented with pink boxes, while light pink boxes represent the 5' and 3' UTRs. On the 6B region, areas with sequence similarity to exon 2 and UTRs of *TaMRC-A1* are indicated, as well as the location of *gypsy* retrotransposons. The locations of the mutations in the *mrc* mutants are depicted with red arrows, and the mutated codons/amino acids are shown in red letters. Large black arrowheads show where the sequence has been truncated for illustration - the length of truncated sequence is indicated above. **C)** Summary of species analysed for the loss of *MRC-B1* during wheat hybridisation

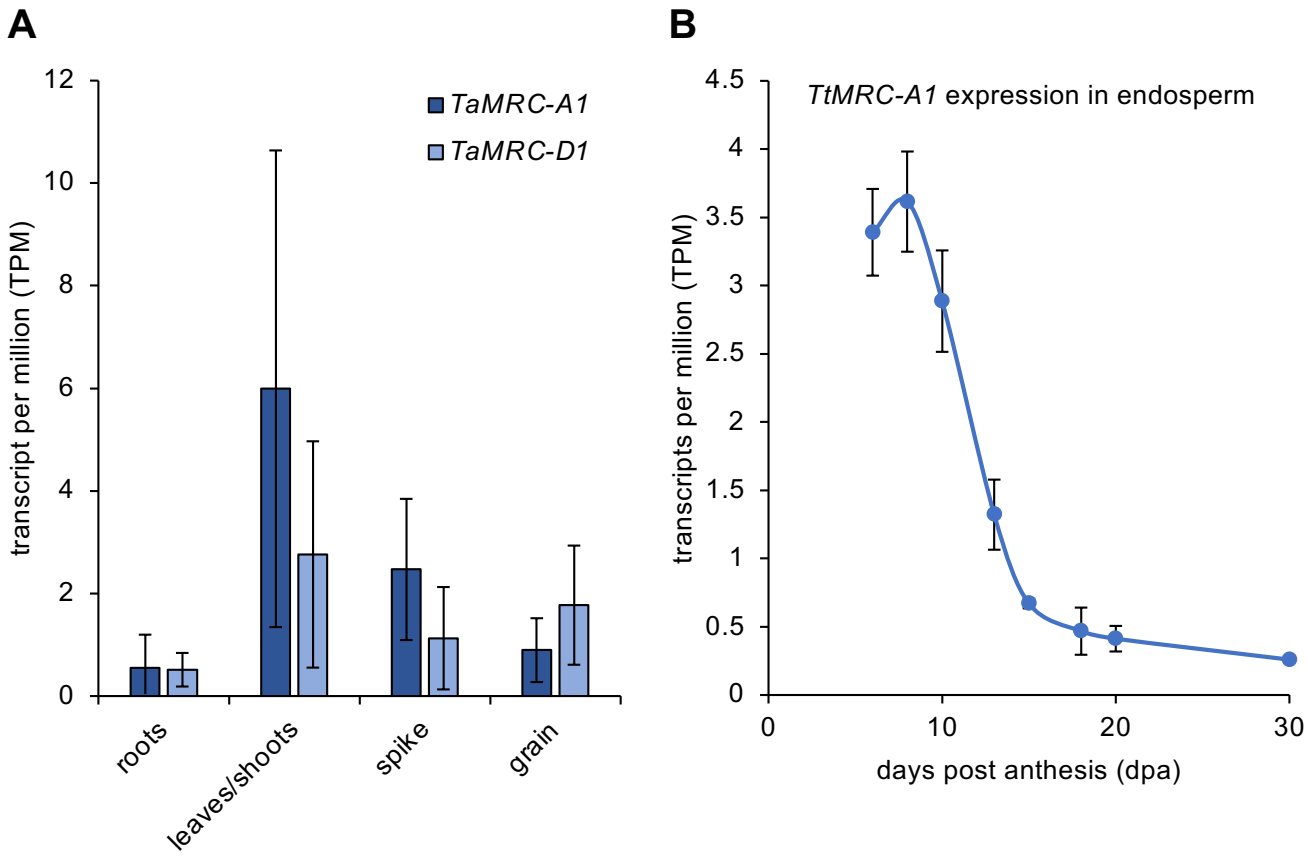

Figure 2. *MRC* is expressed in wheat leaves and wheat endosperm during early grain development. A) Expression of *TaMRC* homeologs between between different tissue types in *Triticum aestivum*. Data were obtained from the wheat expression browser, and values represent transcript per million (TPM) ± SEM from $n = 89$ (roots), 48 (leaves/shoots), 280 (spike), 166 (grain) samples from different experiments. **B)** Expression of *TtMRC-A1* (TRITD6Av1G081580.1) in the starchy endosperm during grain development of *Triticum turgidum* (variety Kronos). Data are from an RNAseq experiment described in Chen *et al.* (2022). Values represent TPM ± SEM from $n = 3$ for all timepoints.

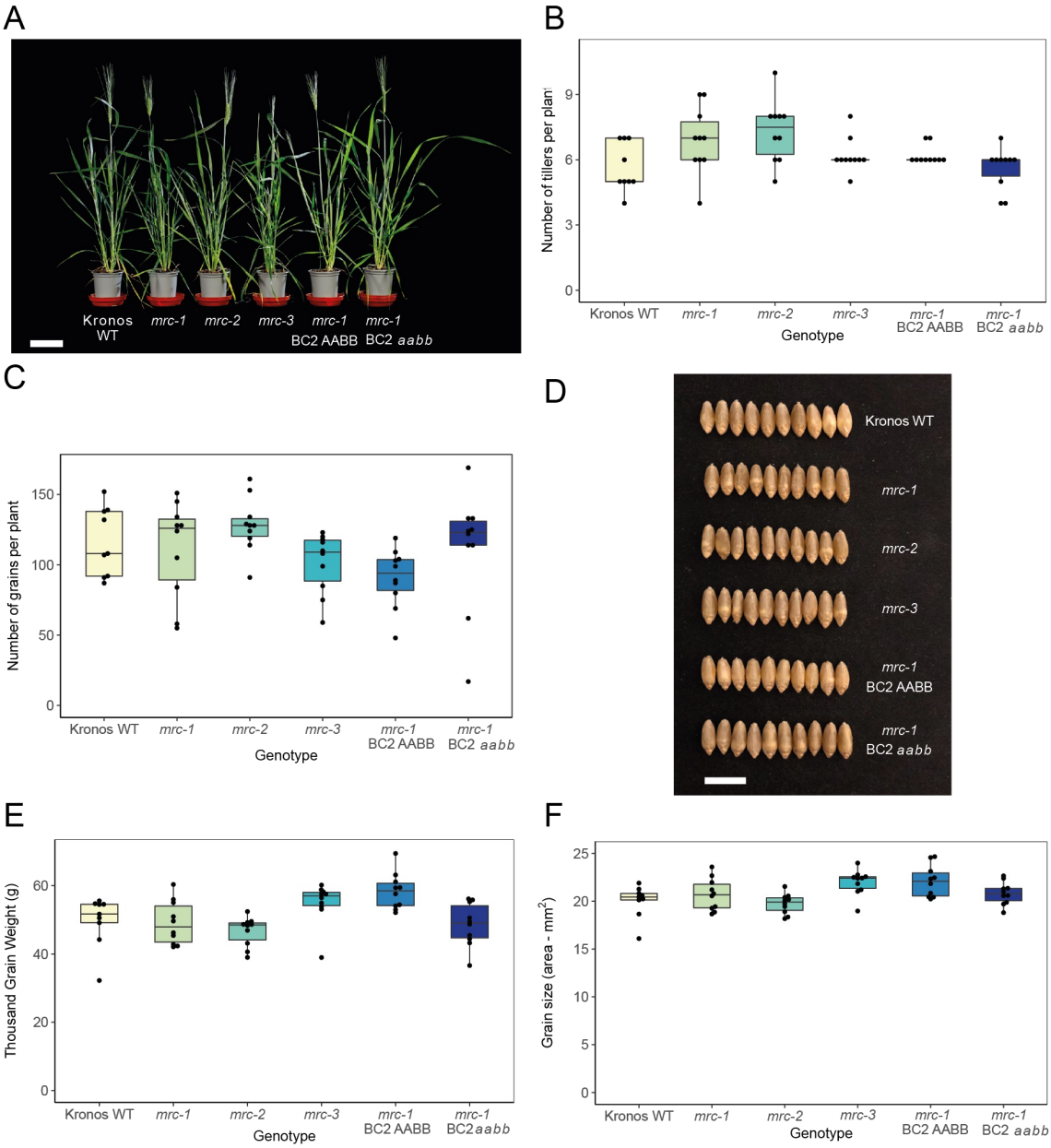

Figure 3. Mutations in *MRC* do not affect plant growth or the number and size of grains. A) Photographs of 7-week-old wild type (WT) and *mrc* mutant plants. Bar = 9 cm. **B)** Number of tillers per plant. **C)** Number of grains per plant. **D)** Photographs of mature grains. Bar = 1 cm. **E)** Thousand Grain Weight (TGW) of mature grains. **F)** Grain size, measured as the average area of individual mature grains from each plant. For statistical analysis of B, C, E, F, see Supplemental Table 1. For all boxplots, each box encloses the middle 50% of the distribution, the middle line is the median and the whiskers are the minimum and maximum values within 1.5 of the interquartile range. Dots are measurements from individual plants, with the same group of plants measured for all phenotypes and $n = 9 – 10$ individual plants.

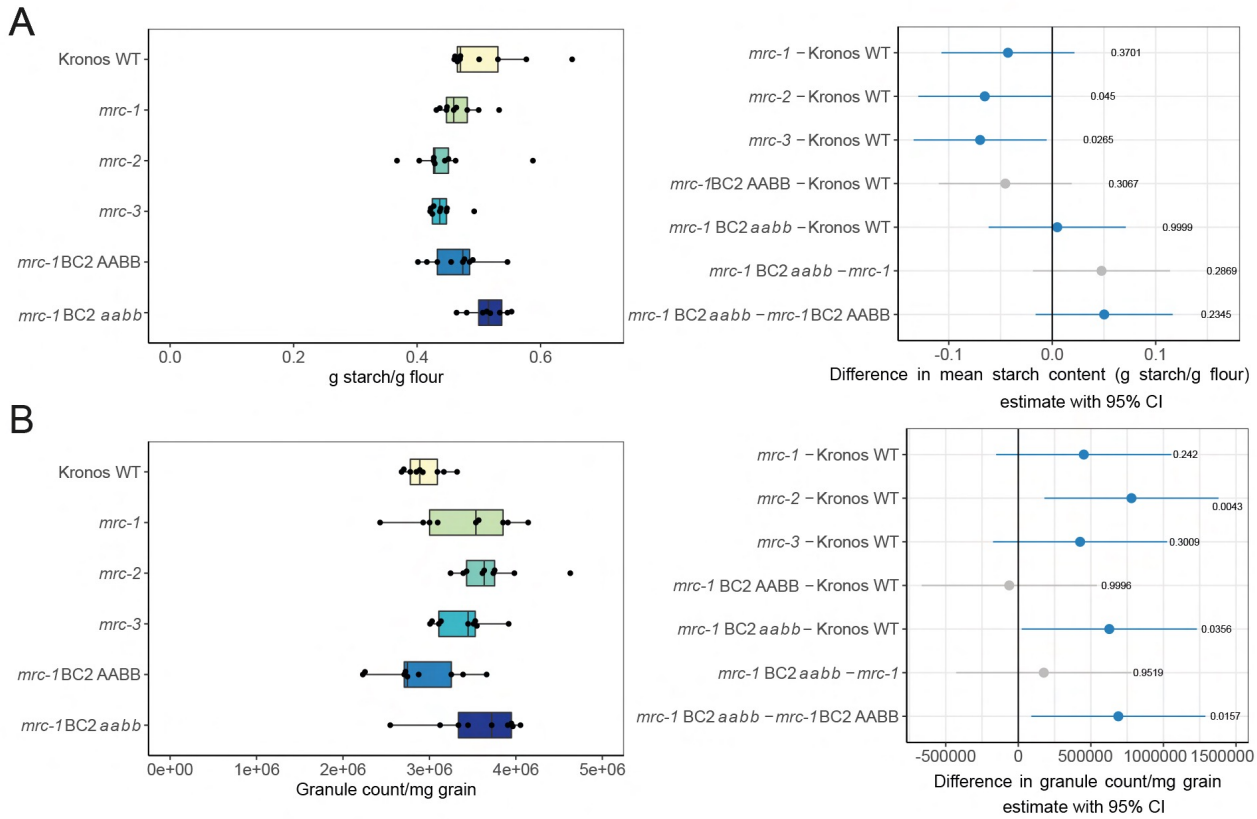

Figure 4. Mutations in *MRC* have variable effects on total starch in mature grains. A) Total endosperm starch content in mature grains in WT and *mrc* mutants. B) Number of starch granules per mg of grain, counted with a Coulter counter. For A and B, dots on the boxplots indicate individual plants, with $n = 8 - 9$. Each box encloses the middle 50% of the distribution, the middle line is the median and the whiskers are the minimum and maximum values within 1.5 of the interquartile range. All statistical analyses were performed using a linear model, with a one-way ANOVA and Tukey post-hoc test. Panels on the right indicate differences in means between genotypes from pairwise comparisons based on these models. The difference in means is indicated by a dot, with whiskers showing the 95% confidence interval (CI) of this difference, with the corresponding p-value. Grey indicates the WT or *mrc-1* mutant compared to the backcrossed line with the equivalent genotype at the *MRC* loci, and blue indicates all other pairwise comparisons.

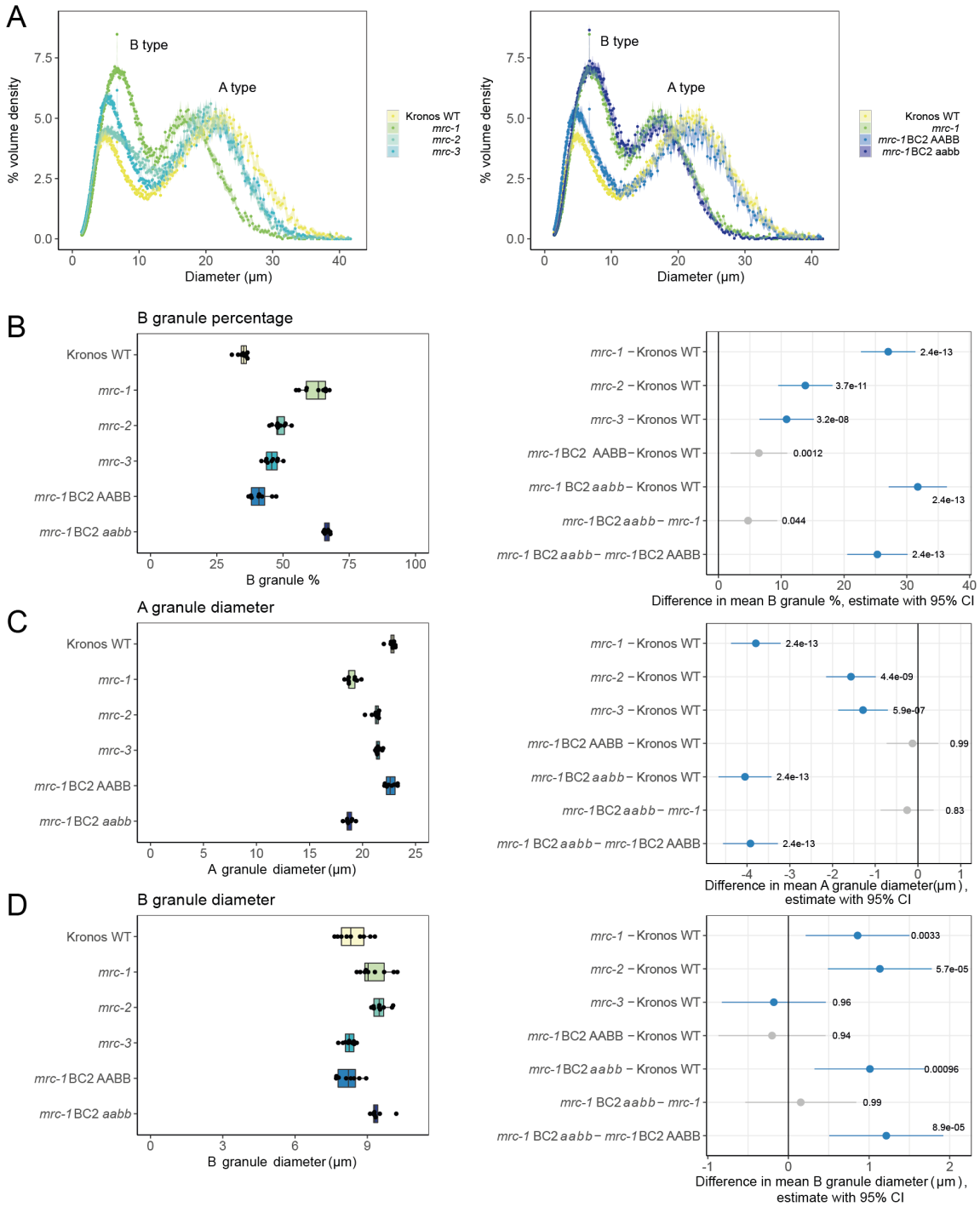

Figure 5. Endosperm starch in mature grains of *mrc* mutants have altered granule size distribution. A) Coulter counter traces with evenly binned x-axes show a bimodal distribution of granule sizes from purified wheat endosperm starch. Data points are mean values from 9 individual plants of each genotype (3 grains from each plant), with the standard error of the mean shown as a shaded ribbon. WT and *mrc-1* in the left and right panel are the same data. **B, C, D)** Mean B-type granule percentage volume (B), A-type granule diameter (C) and B-type granule diameter (D) values extracted from bimodal log-normal distribution curves fitted to Coulter counter traces of individual plants. Extracted values and boxplots are shown on the left, where dots indicate mean values from individual plants (n = 9). Each box encloses the middle 50% of the distribution, the middle line is the median and the whiskers are the minimum and maximum values within 1.5 of the interquartile range. All statistical analyses were performed using linear models for each panel, with a one-way ANOVA and Tukey post-hoc test. Panels on the right indicate differences in means between genotypes from pairwise comparisons based on these models. The difference in means is indicated by a dot, with whiskers showing the 95% confidence interval (CI) of this difference, with the corresponding p-value. Grey indicates the WT or *mrc-1* mutant compared to the backcrossed line with the equivalent genotype at the *MRC* loci, and blue indicates all other pairwise comparisons.

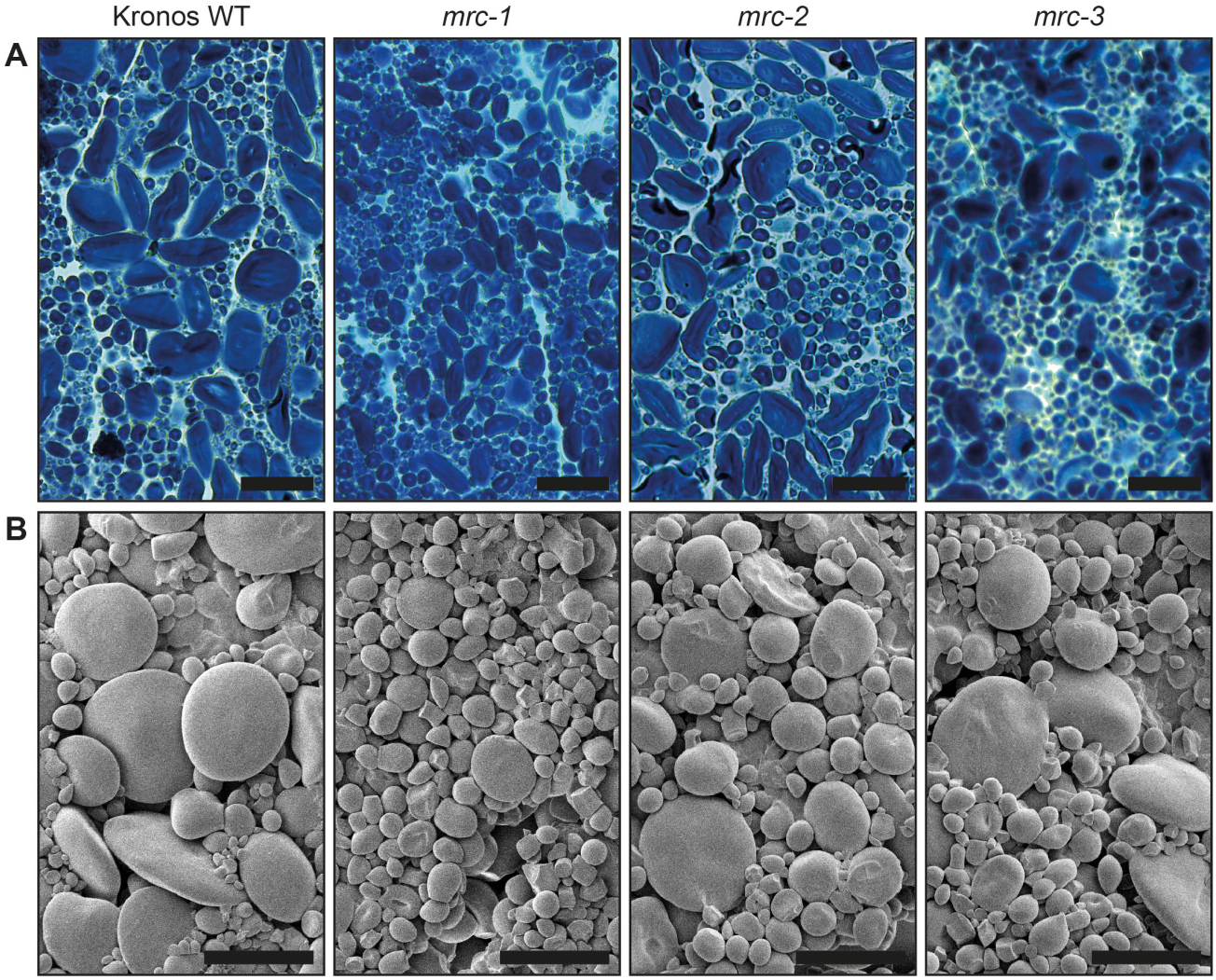

Figure 6. Endosperm starch granules of mature grains in three wheat *mrc* mutants are similar in shape compared to wild type. A) Thin sections of mature endosperm tissue were stained with Lugol's solution and imaged using light microscopy. Bar = 40 µm. **B)** Purified endosperm starch granules were observed using scanning electron microscopy (SEM). Bar = 20 µm.

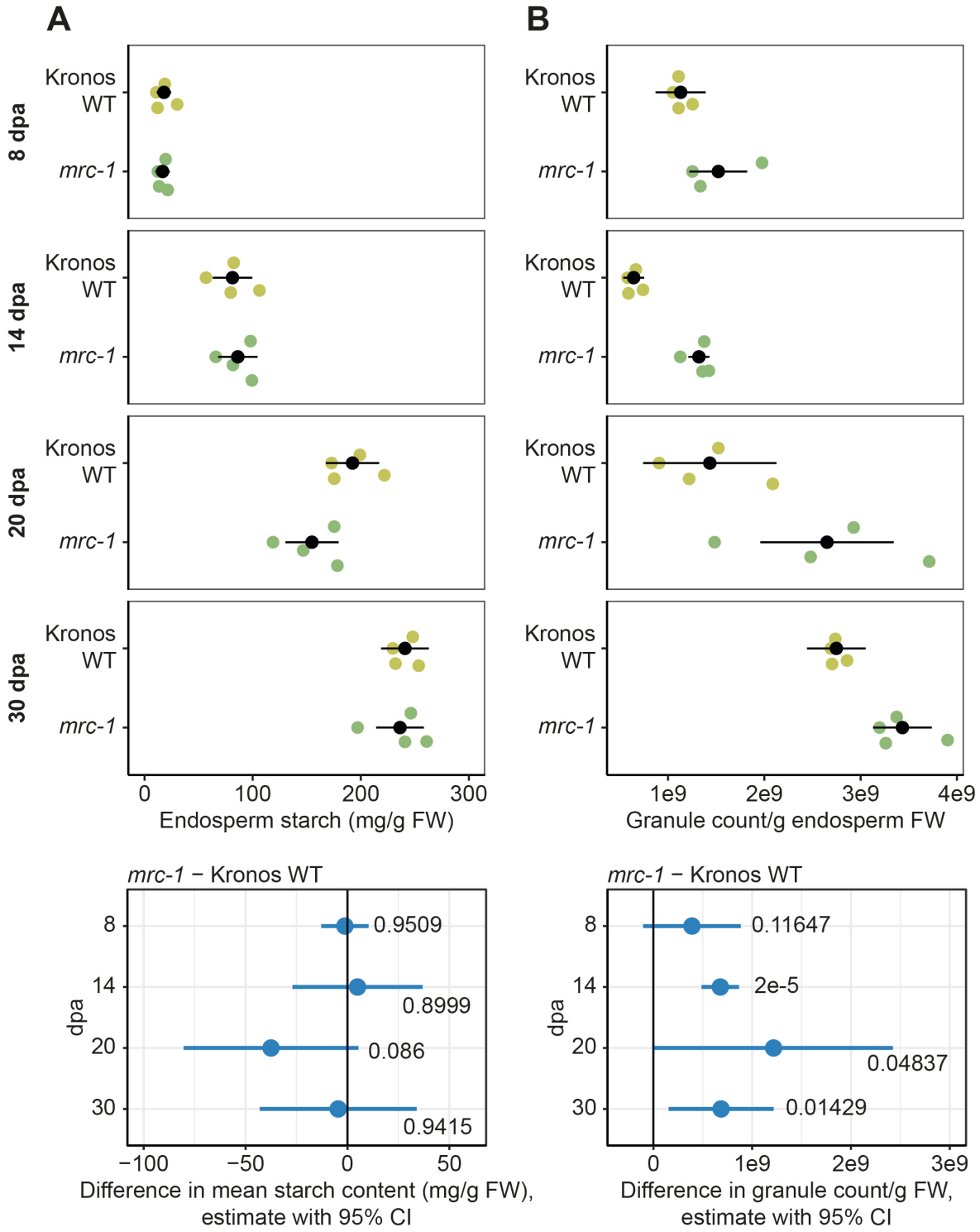

Figure 7. In developing endosperm, granule number increases in *mrc-1* compared to WT despite having similar starch content. The endosperm was dissected from developing grains of WT and *mrc-1*, harvested at 8, 14, 20 and 30 dpa, with n = 3 - 4 individual plants for each genotype per time point, indicated by coloured dots in the upper panels, with the mean ± 95% confidence interval (CI) in black dots and whiskers. **A)** Starch content of the endosperm. Values are expressed relative to the fresh weight of the dissected endosperm. **B)** Starch granule number in the endosperm. Starch was purified from dissected endosperm and the number of granules was determined using a Coulter counter. Values are expressed relative to the fresh weight of the dissected endosperm. For A and B, individual linear models were fitted to the data of each time point, with a one-way ANOVA and Tukey post-hoc test to compare the means of WT and *mrc-1*. Panels on the bottom summarise the differences in means from these linear models, indicated by a dot, with whiskers showing the 95% CI of this difference, with the corresponding p-value.

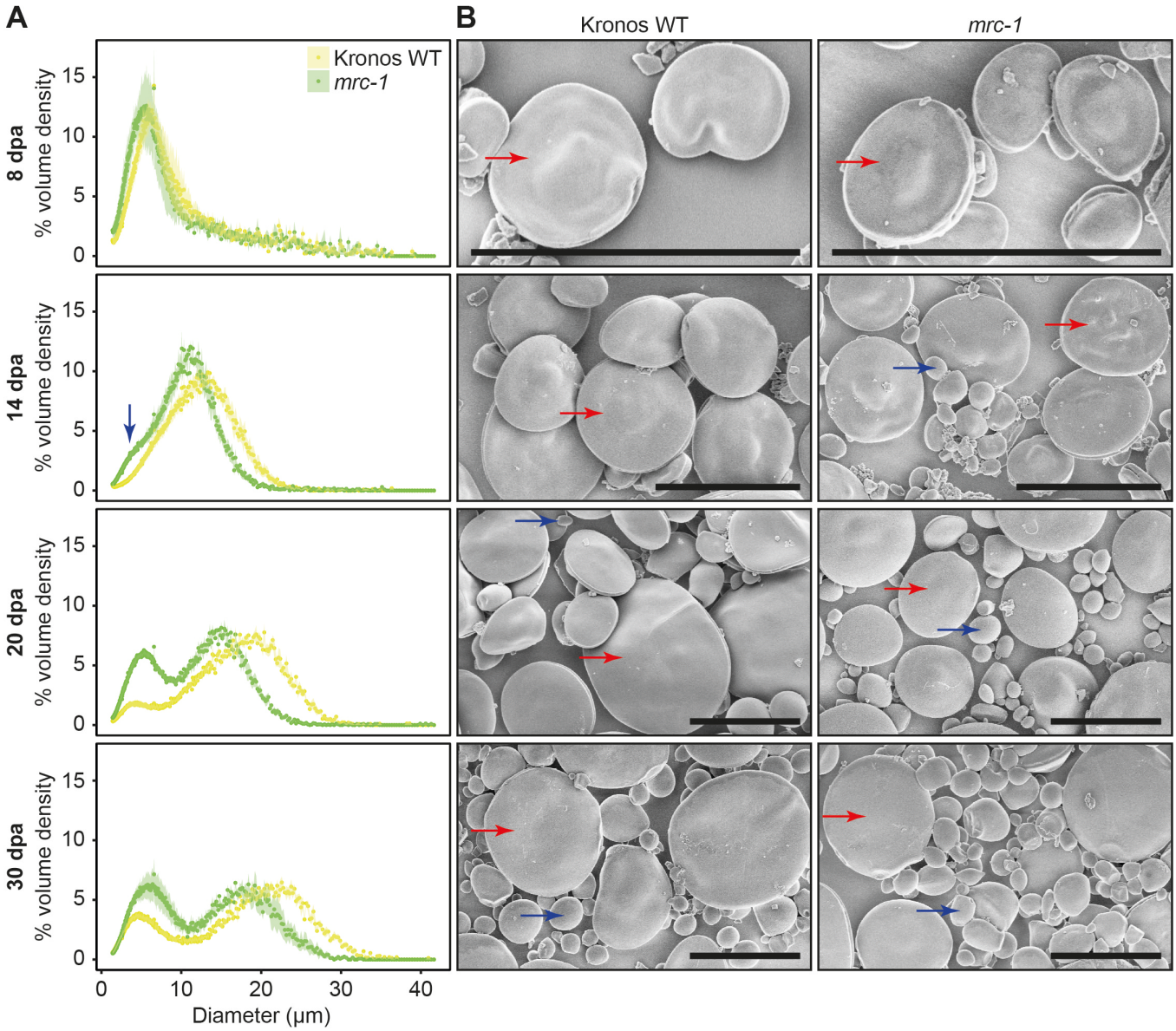

Figure 8. The *mrc-1* mutant initiates B-type granules earlier in grain development than in the wild type (WT). The endosperm was dissected from developing grains of WT and *mrc-1* harvested at 8, 14, 20 and 30 dpa. **A)** Coulter counter traces with evenly binned x-axes show the starch granule size distribution of endosperm starch. Distributions are the average of $n = 4$ measurements, each carried out on grains harvested from a different plant (three grains per measurement). Data points are mean values from these 4 measurements, with the standard error of the mean shown as a shaded ribbon. The B-type granule peak in the *mrc-1* mutant at 14 dpa is indicated with a blue arrow. **B)** Endosperm starch granules were observed using scanning electron microscopy (SEM). Bars = 20 µm. Examples of A-type granules and B-type granules are marked with red and blue arrows respectively.

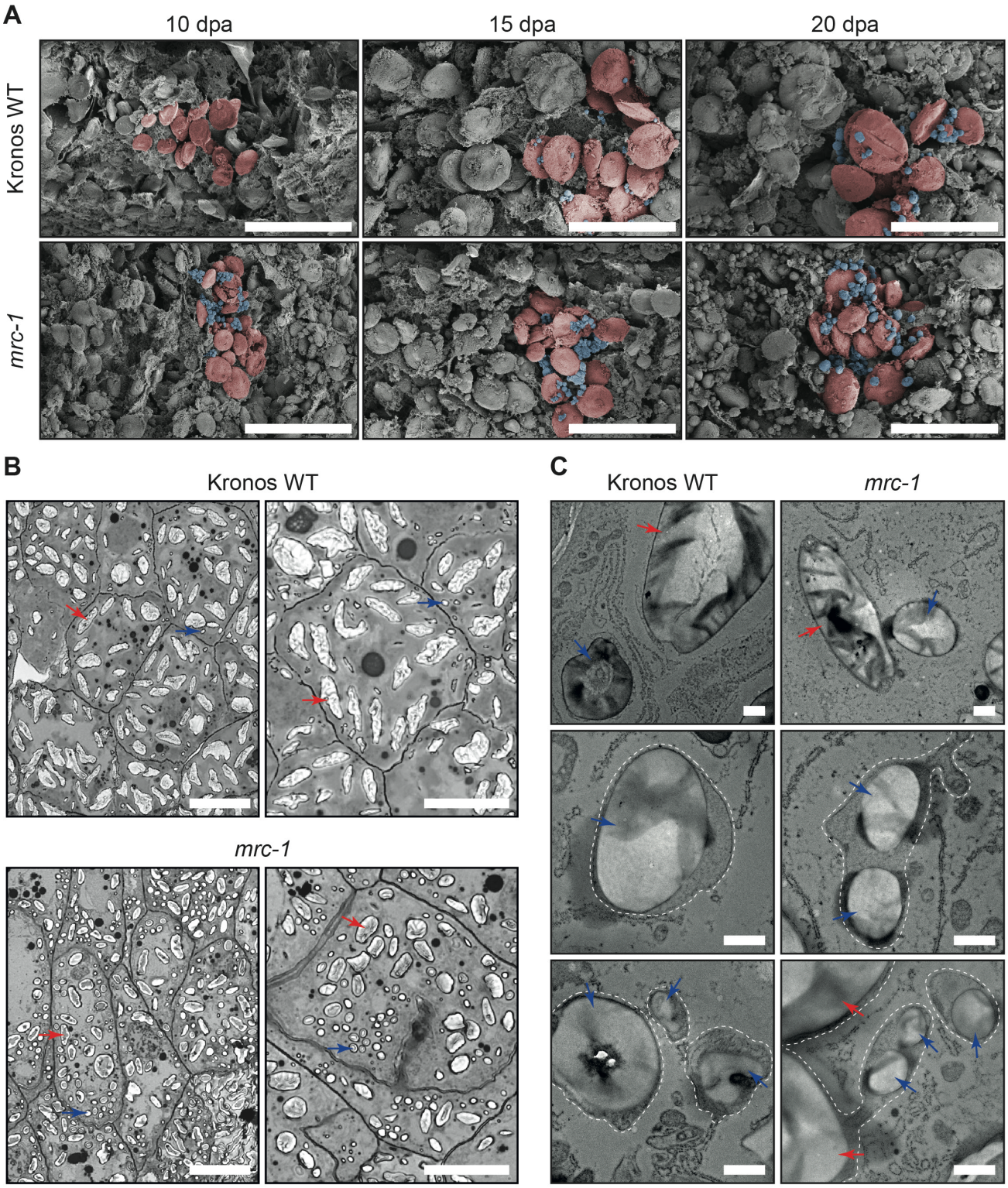

Figure 9. The early initiating B-type granules in *mrc-1* occur at least partially in stromules. A) Scanning electron micrographs of developing endosperm tissue subjected to critical point drying. Grains were harvested from WT and *mrc-1* at 10, 15 and 20 days post anthesis (dpa). A representative region of each panel has been pseudo-coloured, with A-type granules in red shading and B-type granules in blue shading. Bars = 50 µm. **B)** Light micrographs of endosperm sections. Semi-thin sections of embedded developing grains (15 dpa) were stained with toluidine blue as a negative stain for starch granules. Examples of A-type granules and B-type granules are marked with red and blue arrows respectively. Bars = 50 µm. **C)** Endosperm sections observed using transmission electron microscopy, using the same samples as in B. The periphery of amyloplast membranes, where visible, are indicated with a dotted white line. Bars = 1 µm.

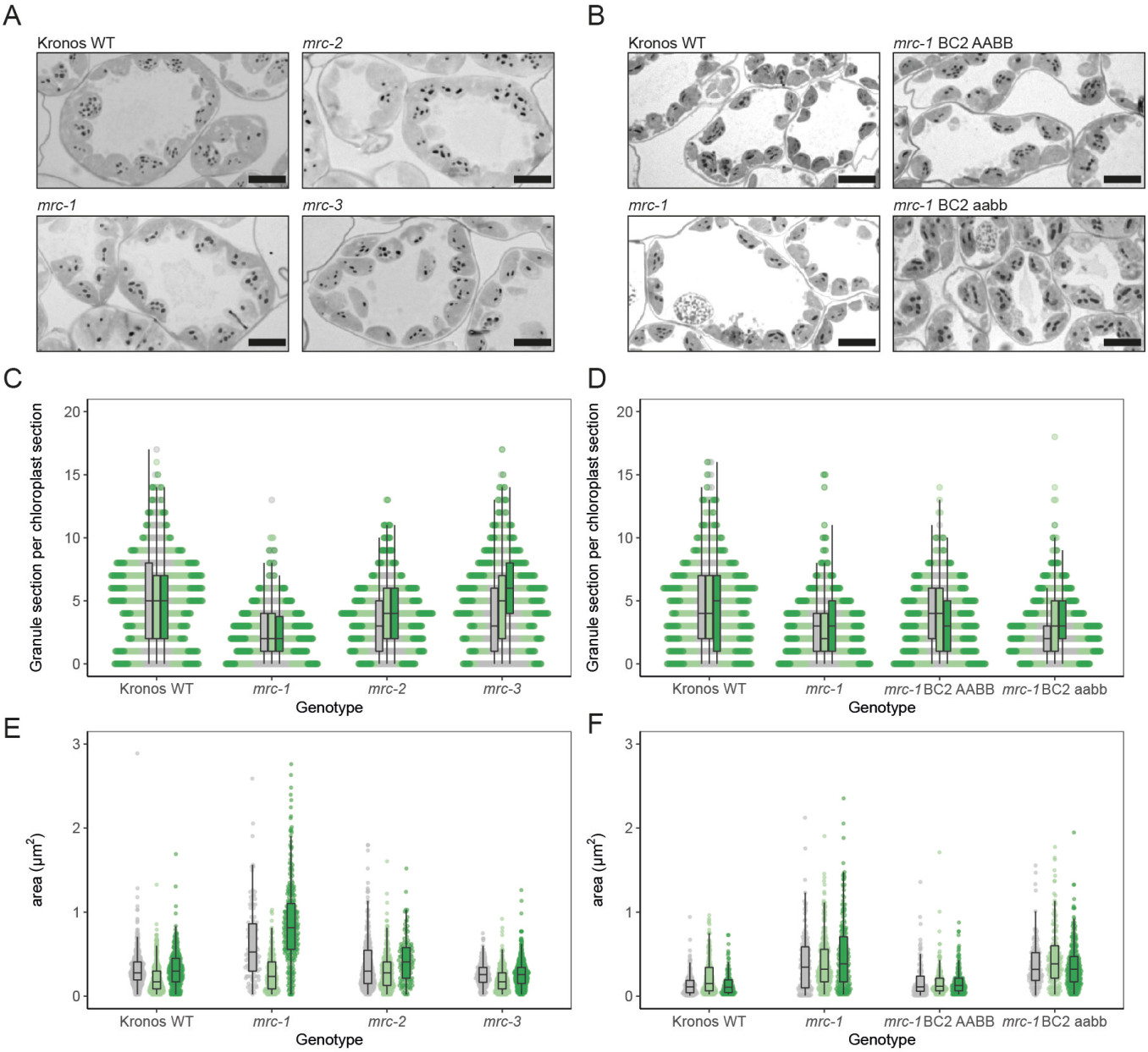

Figure 10. Chloroplasts of *mrc-1* mutants have fewer and larger granules than the wild type. A, B) Representative light microscopy images of thin sections (500 nm) from the middle of the older of two leaves in 10-day old wheat seedlings, collected at the end of day. Sections were stained for starch using periodic acid and Schiff staining. Scale bar = 10 µm. **C, D)** Distributions of counts of granule sections per chloroplast section, counted from light microscopy images as in A and B. The three different colours correspond to three individual plants of each genotype, per experiment. For each sample, 200 – 250 chloroplasts were counted, with absolute values varying between samples. Dots represent individual chloroplasts. **E, F)** Distributions of starch granule sizes measured as the area in the light microscopy images as in A and B. The three different colours correspond to three individual plants of each genotype, per experiment. 100 – 400 granules were measured in each sample. Dots represent individual granules. For all boxplots, each box encloses the middle 50% of the distribution, the middle line is the median and the whiskers are the minimum and maximum values within 1.5 of the interquartile range. Measurements were made on the same batch of plants as Figure 11, experiment 2 (panels A, C, E here) and experiment 5 (panels B, D, F here).

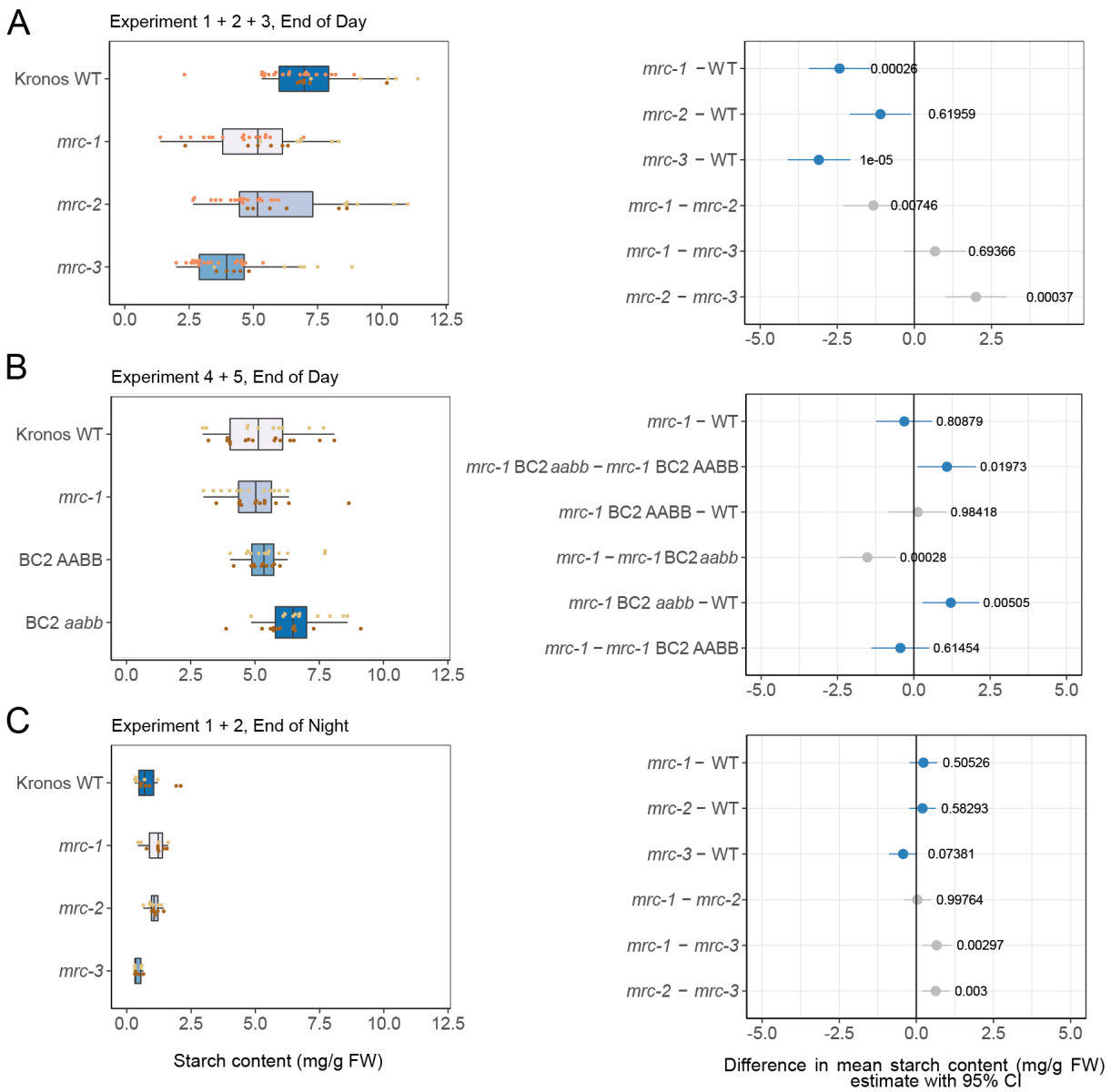

Figure 11. Loss of MRC has variable effects on the total end of day (ED) leaf starch content in wheat leaves. A) Pooled starch content data of wheat leaves harvested at the end of day (ED) in experiments 1 (dark brown, $n = 5 – 6$ per genotype), 2 (light brown, $n = 5 – 6$ per genotype) and 3 (orange, $n = 16 – 19$ per genotype). **B)** Pooled starch content data from wheat leaves in experiments 4 (dark brown, $n = 10 – 15$ per genotype) and 5 (light brown, $n = 10 – 12$ per genotype) harvested at ED. **C)** Pooled starch content data of wheat leaves harvested at the end of night (EN) in experiments 1 (dark brown, $n = 4 – 6$ per genotype) and 2 (light brown $n = 4 – 6$ per genotype) **For all panels**, raw data and boxplots are shown on the left, where dots indicate values from individual wheat plants, with colours indicating each experiment. Each box encloses the middle 50% of the distribution, the middle line is the median and the whiskers are the minimum and maximum values within 1.5 of the interquartile range. All statistical analyses were performed using a linear model with genotype and experiment as fixed effects for each panel, ANOVA and Tukey post-hoc tests. Panels on the right indicate differences in adjusted means of total starch content based on these models and pairwise comparisons of the genotypes. The difference in means is indicated by a dot, with whiskers showing the 95% confidence interval (CI) of this difference, with the corresponding p-value. For A and C, blue indicates comparisons between mutant and wild type, while grey indicates comparisons between mutants. For B, grey indicates the WT or *mrc-1* mutant compared to the backcrossed line with the equivalent genotype at the *MRC* loci, and blue indicates all other pairwise comparisons.

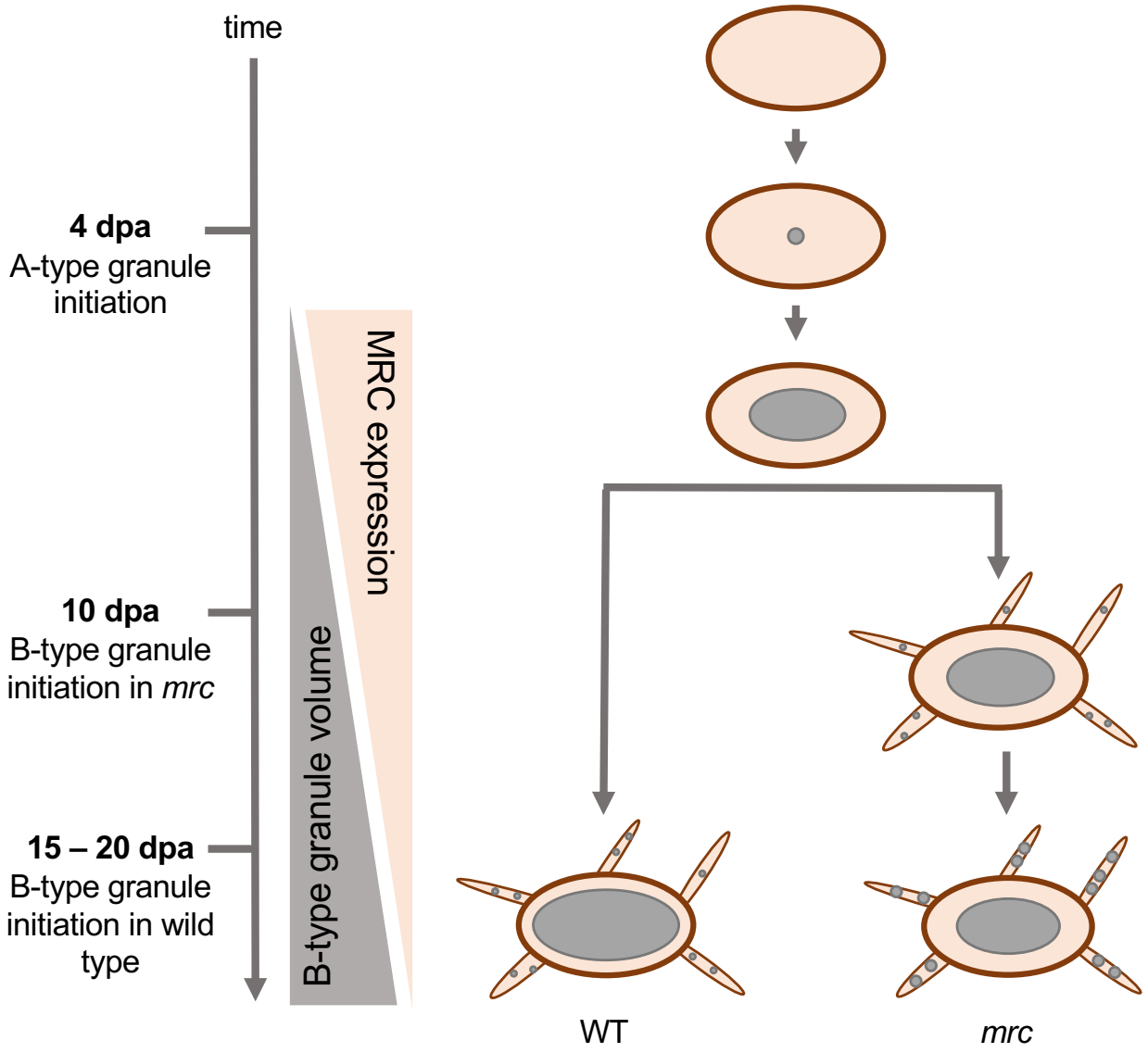

Figure 12. Model of MRC function in wheat developing endosperm. MRC is required for the control of the timing of B-type granule initiation during early grain development. In wild type, A-type granules initiate around 4 days post anthesis (dpa), and B-type granules initiate around 15 – 20 dpa. We propose that the expression of MRC during early endosperm development prevents the B-type granule formation, and B-type granule volume increases as MRC expression decreases after 10 dpa. This process is disrupted in mutants lacking a functional MRC protein, and granules initiate already from 10 dpa. The early initiation of B-type granules provides them with more time and substrate to grow, leading to higher volume of B-type granules in the mutant at grain maturity compared to the wild type, and a concomitant decrease in A-type granule size in the mutant.